1-1-2006

Characterizaton of Nb75Ta for Hix decomposition process

Venkateswarlu Kondur
University of Nevada, Las Vegas

CHARACTERIZATION OF Nb7.5Ta FOR HI_X DECOMPOSITION PROCESS

by

Venkateswarlu Kondur

Bachelor of Technology in Mechanical Engineering
J.N.T.U, Hyderabad, India
May, 2003

A thesis submitted in partial fulfillment
of the requirement for the

Master of Science Degree in Mechanical Engineering
Department of Mechanical Engineering
Howard R. Hughes College of Engineering

Graduate College
University of Nevada, Las Vegas
December 2006

UNLV
UNIVERSITY OF NEVADA LAS VEGAS

Thesis Approval

The Graduate College
University of Nevada, Las Vegas

17th November, 2006

The Thesis prepared by

Venkateswarlu Kondur

Entitled

Characterization of Nb7.5Ta for HI_x Decomposition Process

is approved in partial fulfillment of the requirements for the degree of

Master of Science in Mechanical Engineering

Examination Committee Chair

Dean of the Graduate College

Examination Committee Member

Examination Committee Member

Graduate College Faculty Representative

ABSTRACT

Characterization of Nb7.5Ta for HI_x Decomposition Process

by

Venkateswarlu Kondur

Dr. Ajit K.Roy, Examination Committee Chair
Associate Professor of Mechanical Engineering
University of Nevada, Las Vegas

Nb7.5Ta, a candidate refractory material for use in the HI_x decomposition process, has been tested for evaluation of its tensile properties and corrosion resistance. The results of tensile testing within a temperature range of ambient to 400°C revealed a gradual drop in tensile strength with increasing temperature. However, reduced failure strain was observed at temperatures up to 300°C, suggesting the occurrence of dynamic strain aging (DSA) behavior. The characterization of the tensile specimens by transmission electron microscopy showed somewhat higher dislocation density at 300°C that could be the result of the DSA effect. Corrosion studies under a slow strain rate condition in an acidic solution exhibited enhanced cracking tendency at 90°C, suggesting a detrimental effect of higher temperature on the cracking susceptibility. No failures were observed under a constant-load condition. An application of a cathodic controlled potential to the test specimen resulted in enhanced cracking tendency in terms of failure strain. The morphology of failure, determined by a scanning electron microscope, was ductile in all tested specimens.

TABLE OF CONTENTS

LIST OF FIGURES

LIST OF TABLES

ACKNOWLEDGMENTS

I would like to express my sincere gratitude to my advisor and committee chair, Dr. Ajit K. Roy for his advice, guidance and continuous motivation throughout this research. It was a great pleasure for me to conduct this research work under his supervision.

I am thankful to Dr. Anthony E. Hechanova, Dr. Daniel P. Cook, Dr. Edward S. Neumann, and other faculty members for their valuable suggestions and support throughout this investigation.

I am also thankful to my colleagues at the Material Performance Laboratory for their continuous support during my research work.

I would like to thank my parents, sister and brother-in-law for their encouragement and support, without which this work could not be accomplished. Also, I would like to thank my friends for their inspiration and moral support.

Finally I would like to thank the U.S. Department of Energy for financial support of this Project under grant number DE-FC07-04ID14566.

CHAPTER 1

INTRODUCTION

The extensive use of oil and gas in the past decade had been gradually reducing their supplies and causing crisis due to the imbalance in their supply and demand. The continued depletion of these energy sources has led to a significant escalation in their prices. Further, they have been known to cause global warming due to the generation of CO_2. A combination of both high prices and environmental concerns has prompted many nations to develop alternate sources of energy that must be clean, environment-friendly and cost-effective. Hydrogen is known to be one such source yet to be developed in the United States for commercial applications. Although a number of methods exist to produce hydrogen in a cost-effective manner, a majority of them require high temperature that can only be supplied from very high heat sources.

In order to meet a challenging task of developing an alternate source of energy in a cost-effective manner, the United State Department of Energy (USDOE) has been considering both electrolysis and thermochemical processes using nuclear power as a potential source of heat. However, from the efficiency point of view, the thermochemical[1] processes involving chemical reactions at elevated temperatures appear to be more reasonable and attractive to USDOE. The thermochemical processes currently being envisioned are sulfur-iodine (S-I) and calcium-bromine (Ca-Br) cycles. However, USDOE is leaning towards the S-I process since the Ca-Br cycle is in immature stage.

A schematic view of hydrogen generation using nuclear heat is illustrated in Figure 1.1, showing the transfer of heat from a gas-cooled nuclear reactor through an intermediate heat-exchanger (IHX) into the hydrogen generation plant, where chemical reactions will take place according to the S-I process. The S-I cycle, initially developed by the General Atomics Corporation (GA) of San Diego, California, consists of three chemical reactions that can sum to the dissociation of water using iodine (I_2) and sulfur dioxide (SO_2) as chemical catalysts, as illustrated in Figure 1.2[2]. The reactions occurring in the hydrogen generation plant consists of three steps including the formation and separation of sulfuric acid (H_2SO_4) and hydrogen iodide (HI), concentration and decomposition of H_2SO_4, and HI concentration and decomposition. These chemical reactions [3] are given in the next page.

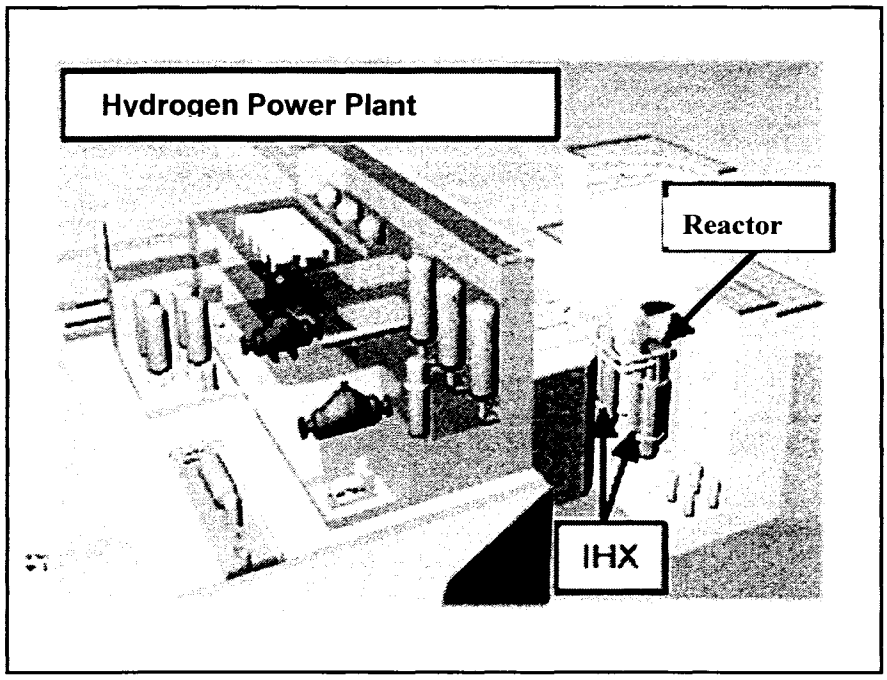

Figure 1.1. Nuclear Hydrogen Generation Plant

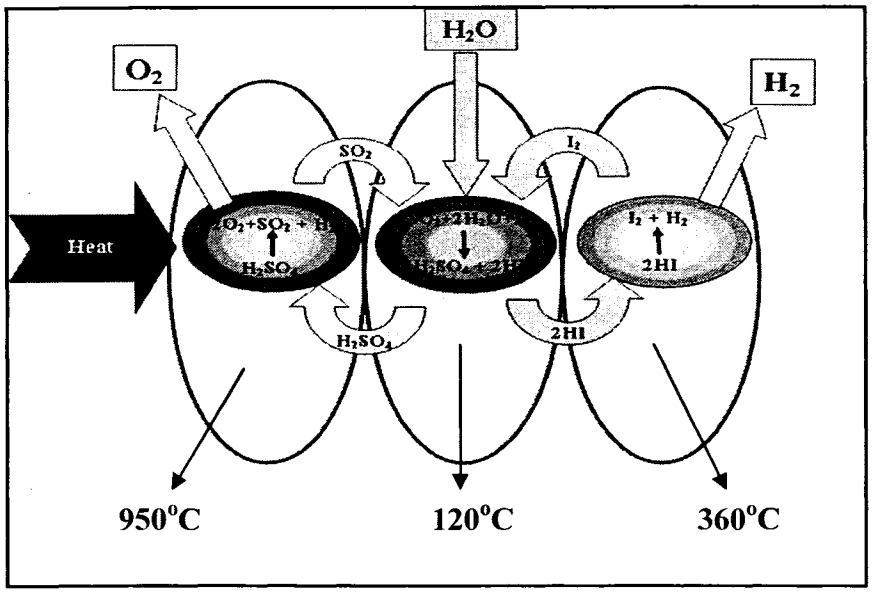

Figure 1.2. Sulfur – Iodine Cycle

$$I_2 + SO_2 + 2H_2O \rightarrow 2HI + H_2SO_4 \qquad \text{(Temperature ~ 120°C)}$$

$$H_2SO_4 \rightarrow H_2O + SO_2 + \tfrac{1}{2}O_2 \qquad \text{(Temperature ~ 950°C)}$$

$$2HI \rightarrow H_2 + I_2 \qquad \text{(Temperature ~360°C)}$$

$$H_2O \rightarrow H_2 + \tfrac{1}{2}O_2$$

As illustrated in Figure 1.2, water reacts with I_2 and SO_2 to form HI and H_2SO_4, which are then separated from each other. I_2 and SO_2 are recovered as byproducts resulting from the breakdown of HI and H_2SO_4, and recycled. Hydrogen (H_2) and oxygen (O_2) gases are subsequently collected separately. As shown in the above reactions, the thermal decomposition of H_2SO_4 is proposed to occur at temperature approaching 950°C. However, the decomposition of HI into H_2 and I_2 occurs at a relatively lower temperature of 400°C by extractive distillation that involves heating of hydroiodic acid (HI_x), which eventually decomposes into H_2 and I_2 at the top of the reactive column. While this

technique of hydrogen generation involves less processing equipment, it can still create a highly corrosive environment (pH ~ 1 or less) at relatively high temperature (400°C) and pressure (70 bar). Therefore, the structural materials to be used to generate hydrogen from the decomposition of HI must be highly corrosion-resistant and should have adequate structural strength.

It is obvious from the preceding section that the structural materials to be used in heat-exchangers using the S-I cycle must withstand appreciably high temperature in the presence of hostile chemical species. Thus, the identification and characterization of suitable materials for such applications is a major task. In view of this challenge, an ambitious research project was pursued at the Materials Performance Laboratory, (MPL) of UNLV to characterize the metallurgical and corrosion behavior of suitable candidate structural materials for use under prototypic conditions. The characterization of a few candidate materials is also in progress at GA using a prototypic environment. The Materials Advisory Board formed by USDOE recommended the use of refractory materials including zirconium (Zr), and niobium (Nb) alloys having optimum corrosion resistance and the desired metallurgical properties to sustain the hostile operating conditions relevant to the HIx decomposition process. These materials include Zr7O2, Zr7O5, Nb1Zr and Nb7.5Ta. The experimental data involving the first three alloys have been presented earlier by UNLV researchers [4,5]. This thesis is primarily aimed at presenting the most recent metallurgical and corrosion data obtained on Nb7.5Ta.

Niobium (Nb) and tantalum (Ta) are known to possess excellent corrosion resistance in many chemical environments. Both materials fall under Group V refractory materials and possess high ductility in the pure state. They have relatively high solubility of

interstitial elements including carbon, nitrogen, oxygen and hydrogen, and can exhibit a very low ductile-brittle-transition-temperature (DBTT). Nb possesses a number of desirable properties that make it attractive for nuclear applications and for structural components in aircraft and space vehicles [6]. These properties include high melting point, moderate density, excellent fabricability and a low thermal neutron absorption cross-section. Further, Nb has adequate weldability and plasticity that are needed in the fabrication of structural components. However, it has poor oxidation resistance that can prevent the use of this material in high-temperature engineering applications. In order to improve its high- temperature oxidation resistance, Nb is alloyed with other refractory materials such as Ta that can provide improved tensile and creep properties at elevated temperatures [7].

Ta is ductile, easily fabricated, highly resistant to corrosion in acids and liquid alkali metals, a good conductor of heat and electricity and has a very high melting point. It has a significant corrosion resistance in environments containing a wide spectrum of chemical reagents. The addition of Ta to Nb can enhance the corrosion resistance of this alloy in the presence of many hostile chemical species including fluorides [7]. In view of these rationales, a refractory material containing Nb and Ta, namely Nb7.5Ta was included in this investigation to characterize both the metallurgical and corrosion behavior under conditions relevant to the HI_x decomposition process of the S-I cycle.

Significant efforts have been made in this investigation to determine the tensile properties of Nb7.5Ta at temperatures ranging from ambient to 400°C, which is the maximum operating temperature proposed for the HI_x decomposition process. The tensile properties evaluated include the yield strength (YS), ultimate tensile strength (UTS),

percent elongation (%El), and percent reduction in area (%RA). An interesting observation was made from the resultant tensile data, showing reduced ductility in terms of the failure strain (e_f) in the temperature regime of ambient to 300°C. Beyond 300°C, the magnitude of e_f was enhanced. The reduction in ductility at temperatures up to 300°C in terms of e_f can be attributed to the inhibition of dislocation mobility in the vicinity of the grain boundaries of Nb7.5Ta possibly due to the diffusion of solute elements. At 400°C, the dislocation mobility was enhanced due to the increased plastic flow. Such phenomenon of reduced ductility within a specified temperature range has often been cited[8] to be result of dynamic-strain-aging (DSA) of susceptible materials. The characterization of dislocations has, therefore, been performed by transmission electron microscopy (TEM) that has also been included in his thesis.

Simultaneously, the susceptibility of Nb7.5Ta to different types of environment-assisted degradations including stress corrosion cracking (SCC) and localized corrosion (pitting / crevice) has been determined in an acidic solution. Since, the generation of hydrogen can influence the cracking behavior of this alloy during its exposure in an acidic solution, an effort has been made to study the role of controlled cathodic (negative) potential on its cracking susceptibility. Extensive work has also been performed to characterize the morphology of failures of specimens used in both tensile and corrosion testing using scanning electron microscopy (SEM). In essence, this thesis presents the comprehensive test results with respect to both the metallurgical and environmental aspects of degradations of Nb7.5Ta for prospective applications in the hydrogen generation process under the nuclear hydrogen initiative (NHI) program.

CHAPTER 2

TEST MATERIAL, SPECIMEN AND ENVIRONMENT

It is obvious from the discussion provided in the previous chapter that the structural material to be used in heat-exchangers for hydrogen generation using the S-I cycle must possess sufficiently high structural strength at elevated temperatures and be corrosion resistant in the presence of hostile chemical species such as HI_x. Conventionally, structural strength is determined under tensile loading at a preferred strain rate using cylindrical specimens according to an appropriate technical standard. This type of specimen can also be used in the determination of corrosion resistance of a candidate structural material under different loading conditions. For electrochemical testing, a different configuration of specimen is commonly used. The different types of test specimens and their configurations are presented in this chapter. Further, a detailed discussion on the test material (Nb7.5Ta) will be provided.

2.1 Test Material

The material tested in this investigation is Nb7.5Ta that can optimize the desired properties needed to sustain the hostile operating conditions related to the HI_x decomposition process. Nb alloys are resistant to corrosion in many chemical environments including the presence of acids and alkalis. However, their oxidation resistance at elevated temperatures is very poor unless protective coatings are applied

onto their surface [7]. In order to circumvent the problems associated with poor oxidation resistance of Nb alloys, it is customary to add alloying elements to enhance this property. Ta is one such alloy, which has not only an improved oxidation resistance but also an excellent corrosion resistance, and thermal conductivity along with a high melting point. In view of these superior properties of Ta, Nb is often alloyed with Ta to render this alloy suitable for application in many hostile environments including that of the HI_x decomposition process.

The physical properties of Nb7.5Ta alloy are not available in the open literature. A comparable analysis of these properties has, therefore, been presented in Tables 2.1 and 2.2, for Nb and Ta, respectively [9, 10]. An evaluation of these data clearly suggests that the Ta possesses higher melting and boiling points compared to that of Nb, suggesting a higher resistance to oxidation.

Table 2.1. Physical Properties of Nb

Properties	Temperature, °C	Metric Units
Density	20	8.57 g/cm^3
Melting Point	2468	-
Boiling Point	5127	-
Electrical Resistivity	25	12.5 microhm-cm
Thermal Conductivity	0	52.3 W/m°K
Coefficient of Thermal Expansion	18 – 400	7.39*10^{-6} m/cm/°C
Specific Heat	0	0.064 cal/g/°C

Table 2.2. Physical Properties of Ta

Properties	Temperature, °C	Metric Units
Density	20	16.6 g/cm^3
Melting Point	2996	-
Boiling Point	5425	-
Electrical Resistivity	20	12.5 microhm-cm
Thermal Conductivity	25	57.5 W/m°K
Coefficient of Thermal Expansion	25 – 1400	7.38*10^{-6} m/cm/°C
Specific Heat	0	0.033 cal/g/°C

Nb7.5Ta, tested in this investigation, was procured from a vendor (ATI Wah Chang) in a solution-annealed condition in the form of cylindrical bars. The chemical composition and the vendor-supplied tensile properties of this alloy at ambient temperature are given in Tables 2.3 and 2.4, respectively. No additional thermal treatments were given to these cylindrical bars prior to the sample preparation.

Table 2.3. Chemical Composition of the Test Material (wt %)

Element	Material/Heat #
	Nb7.5Ta/ 580316
C	0.0022
Fe	0.0035
H	0.0003
Hf	0.0030
Mo	0.0030
N	0.0020
Ni	0.0030
O	0.0125
Si	0.0050
Ta	7.44
Ti	0.0030
W	0.0050
Zr	0.0050
Nb	Balance

Table 2.4. Ambient-Temperature Tensile Properties of Nb7.5Ta

Heat No.	Yield Strength, Ksi (MPa)	Ultimate Tensile Strength, Ksi (MPa)	% El
580316	16.5 (113.77)	31 (213.74)	49

2.2 Test Specimens

The tensile properties of Nb7.5Ta were determined by using smooth cylindrical specimens having 4.00-inch (101.6 mm) overall length, 1.00-inch (25.4 mm) gage length and 0.25-inch (6.35 mm) gage diameter. A ratio of 4 was maintained between the gage length and gage diameter according to the dimensional requirements prescribed by the American Society for Testing and Materials (ASTM) Designation E 08 (2004) [11]. These cylindrical specimens were machined from round bars in such a way that the gage section was parallel to the longitudinal rolling direction. The cylindrical specimens were also used in stress corrosion cracking (SCC) testing under different loading conditions. The dimension and a pictorial view of the smooth cylindrical specimen are shown in Figure 2.1.

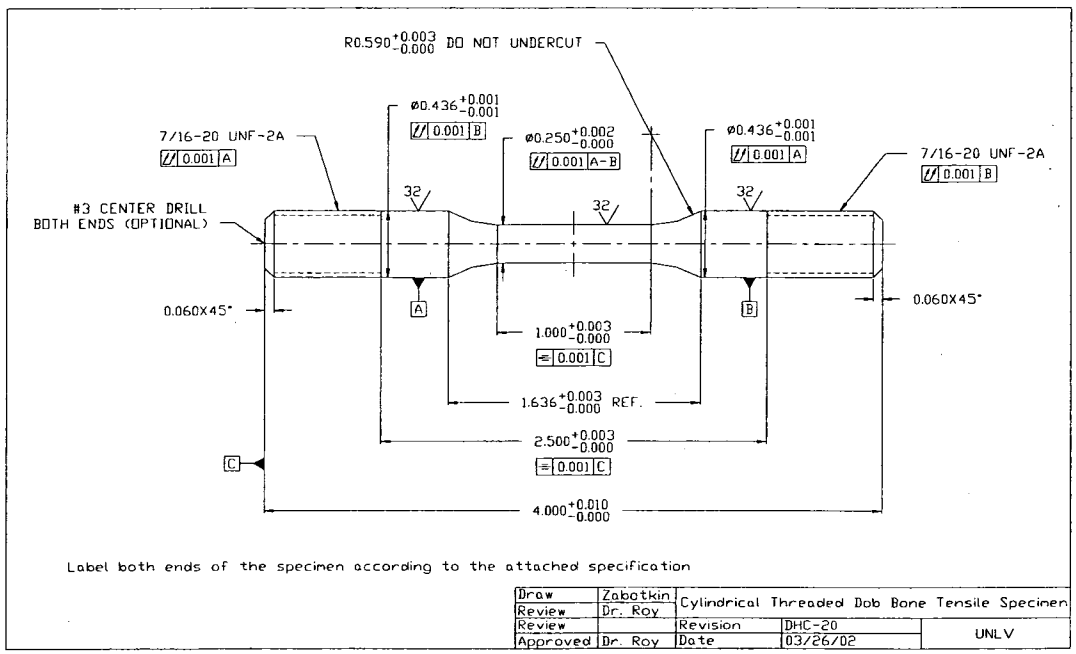

(a) Dimensions

(b) Pictorial View

Figure 2.1. Smooth Cylindrical Specimen

The susceptibility of Nb7.5Ta to localized corrosion (pitting/crevice) was determined by using smaller cylindrical specimens having 0.5-inch (12.7 mm) length and 0.375-inch (9.50 mm) diameter. These specimens also had a central hole for holding it during electrochemical testing with a threaded stainless steel rod. The dimension and a pictorial view of the polarization specimens used in localized corrosion studies are illustrated in Figure 2.2.

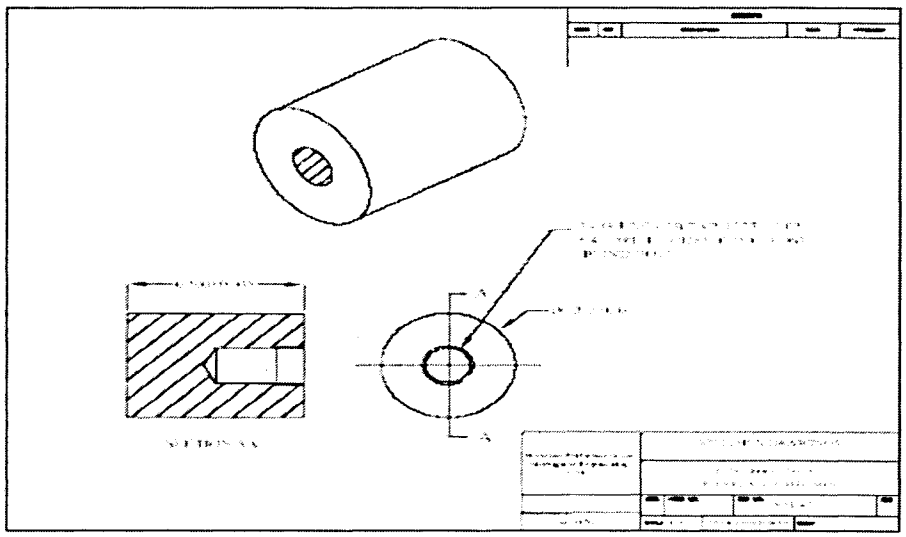

(a). Dimensions

(b). Pictorial View

Figure 2.2. Polarization Specimen

As indicated in the previous chapter, the cracking susceptibility of Nb7.5Ta may be influenced by the presence of hydrogen. Therefore, SCC testing was performed using cylindrical specimens under the influence of hydrogen, generated by applying cathodic electrochemical potential during straining while exposed to the test solution. In order to apply this potential, a conductive stainless steel wire was spot-welded near one of the shoulders of the cylindrical specimen. A pictorial view of a spot-welded cylindrical specimen is shown in Figure 2.3

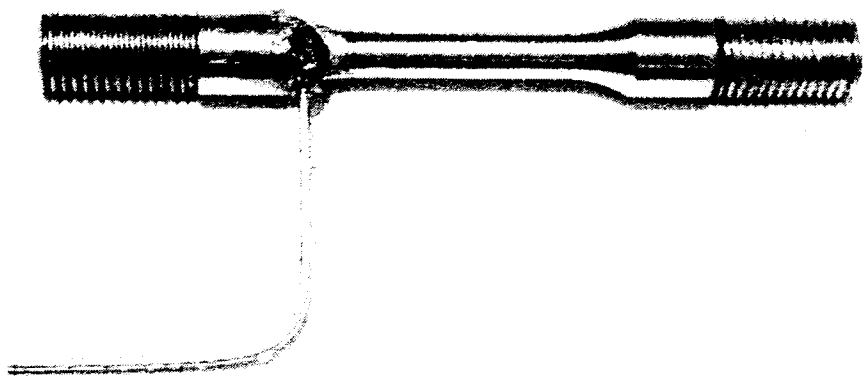

Figure 2.3. Spot Welded Smooth Tensile Specimen

2.3 Test Environment

This investigation is primarily focused on the characterization of Nb7.5Ta for application in the HI_x decomposition process related to the S-I cycle. HI_x is a highly corrosive and toxic environment having an approximate pH of 1 or less. Therefore, corrosion studies involving HI_x could not be accommodated in the Materials Performance Laboratory (MPL). However, Corrosion studies in the HI_x environment are currently being performed at GA research facilities. Simultaneously, an aqueous environment, relevant to the S-I process was used in this investigation that contained de-ionized water, sulfuric acid (H_2SO_4) and sodium iodide (NaI). The chemical composition of this environment is given in Table 2.5

Table 2.5. Chemical Composition of the Test Solution

Test Solution	De-ionized Water, liter	NaI, gm/liter	H_2SO_4, Cc
Acidic solution	1	10	Add sufficient volume to achieve a pH of 1

CHAPTER 3

EXPERIMENTAL TECHNIQUES

As indicated earlier, the maximum temperature for the HI_x decomposition process lies in the vicinity of 400°C. Therefore, the tensile properties of Nb7.5Ta have been determined at temperatures ranging from ambient to 400°C using a conventional testing technique. Since Nb7.5Ta alloy did exhibit a tendency to dynamic-strain-aging (DSA) within a temperature regime of ambient to 300°C, transmission electron microscopy (TEM) was used to determine the dislocation density in specimens tested at ambient temperature, 300°C and 400°C. The susceptibility of this alloy to stress corrosion cracking (SCC) has been evaluated in an acidic aqueous solution using both constant-load (CL) and slow-strain-rate (SSR) testing techniques. Since the presence of hydrogen (H_2) during the HI_x decomposition process can influence the cracking behavior of this alloy, SCC testing was also performed under cathodic (negative) applied potential using the SSR technique. A limited number of electrochemical polarization tests were performed at ambient temperature to determine the corrosion potential of this alloy. The magnitude of the cathodic applied potential was based on the corrosion potential determined from the polarization experiments. The metallurgical microstructures were determined by conventional metallographic technique using an optical microscope (OM). The characteristics of failure of the tested specimens were determined using a scanning

electron microscope (SEM). The different experimental techniques used in this investigation are described in the following subsections.

3.1 Tensile Properties Evaluation

The tensile properties, which include yield strength (YS), ultimate tensile strength (UTS), percent elongation (%El), and percent reduction in area (%RA) were evaluated at temperatures ranging from ambient to 400°C using the MTS model 319.25 testing equipment. This machine had a maximum axial load capability of 250 KN and a torsional load transducer with a maximum capacity of 2200 N-m. The MTS unit was attached to a ceramic-lined heating chamber capable of maintaining temperatures up to 600°C. This equipment had a heavy-duty load-frame connected to an adjustable cross-head on the upper part. A movable hydraulic actuator connected to a wedge grip enabled the fixing of the specimen at the lower end. The axial motion of the cross-head was controlled by force, displacement, or external signal from the strain gage. The specimen attached between the two wedge grips, was pulled by this actuator. The cross-head movement enabled the application of load to the specimen. The magnitude of load was measured by a load cell contained in the cross-head.

The MTS unit was equipped with an 8-channel signal-conditioning box. This signal-conditioning box was used to monitor the strain gages, extensometers, and temperature sensors. The software interface managed all corresponding signals during the testing. A laser extensometer having a scan rate of 100 scans/sec was used to measure the elongation of the gage section. Nitrogen (N_2) was circulated through the heating chamber during the testing at elevated temperatures to avoid the oxidation / contamination of the

specimen surface. The testing temperature inside this chamber was monitored by two K-type thermocouples. The MTS unit is shown in Figure 3.1. The times needed to achieve the desired temperatures during straining under tensile loading are given in Table 3.1.

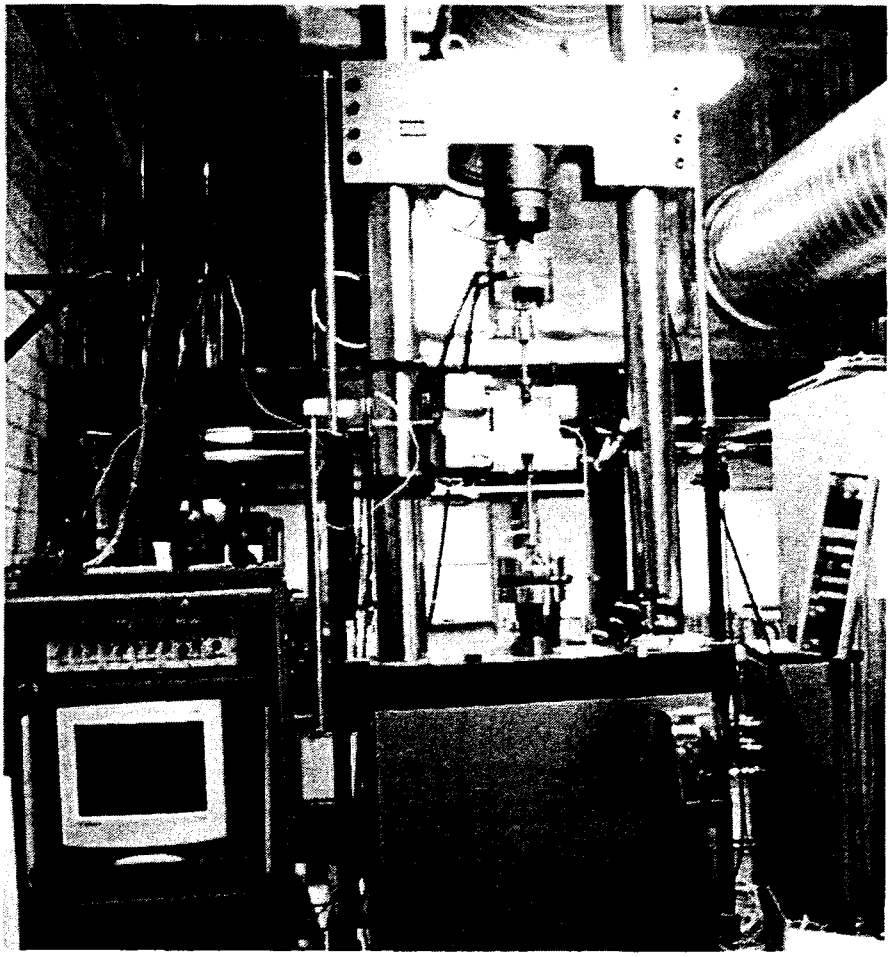

Figure 3.1. MTS Unit

Table 3.1. Calibration Data for the Furnace

Target temperature, °C	Chamber set point temperature, °C	Time to reach the target temperature, min
100	143	60
200	253	60
300	363	60
400	467	55

The smooth cylindrical specimens were loaded in tension by applying a strain rate of $5*10^{-4}$ sec^{-1} according to the ASTM designation E 8 [11]. The experimental data including the load, time and extensometer readings were recorded in a data file at the rate of 100 data points per second. The engineering stress versus strain (s-e) diagrams were developed using these data. The magnitude of YS was determined by the point of intersection of a line drawn parallel to the linear portion of this curve at a strain offset value of 0.2% of strain. The magnitude of UTS was also determined from the s-e diagram. However, the ductility in terms of %El and %RA was determined using the specimen dimensions before and after testing. An average value based on two tests was used to express each parameter obtained from these tensile testing. The magnitude of %El and % RA were determined according to the equations given below.

$$\% \text{ El} = \left(\frac{L_f - L_o}{L_o} \right) \times 100 \qquad \text{(Equation 3.1)}$$

$$\%\text{RA} = \left(\frac{A_o - A_f}{A_o} \right) \times 100 \qquad \text{(Equation 3.2)}$$

$$A_o = \frac{\pi \times D_o^{\,2}}{4} \qquad \text{(Equation 3.3)}$$

$$A_f = \frac{\pi \times D_f^{\,2}}{4} \qquad \text{(Equation 3.4)}$$

where,

A_0 = Initial cross sectional area

A_f = Cross sectional area at failure

L_o = Total Initial length

L_f = Total Final length

D_o = Initial gage diameter

D_f = Final gage diameter

3.2 Defects Characterization by Transmission Electron Microscopy

During tensile testing, an interesting phenomenon occurred, showing reduced failure strain in the temperature regime of ambient to 300°C. The reduced failure strain is an indication of impeding dislocation movement through the metal lattice, thus causing reduced plasticity in terms of the failure strain. This phenomenon of reduced plasticity is attributed to the diffusion of solute elements into the metal lattice, leading to the accumulation of dislocations near the grain boundaries. The formation of dislocations and their movement through the grain boundaries are needed for plastic deformation of structural materials. The reduced plastic strain, as seen in this investigation, is known to be associated with a metallurgical concept termed as DSA. TEM was used to characterize the concentration of dislocations, also known as dislocation density (ρ) of specimens tested within and above the susceptible temperature regime for DSA.

The TEM samples [12] were prepared by cutting sections from the broken cylindrical tensile specimens tested at different temperatures. These sectioned samples had approximate thickness of 300 – 400 μm. Subsequently, they were ground into thin foils of 100 – 150 μm thickness followed by their punching in a mechanical press to form discs having diameters of approximately 3 mm. These thin film discs were then electrolytically polished in a twin-jet apparatus using an etchant consisting of 5 volume percent of perchloric acid in methanol. During electropolishing of these discs, a potential of 50 volts was applied to them at a temperature of -8°C. The step-by-step procedure for preparing these thin film samples are illustrated in Figure 3.2. A TECNAI model G^2 F30 S-TWIN TEM, shown in Figure 3.3, was used to develop micrographs of these thin foils.

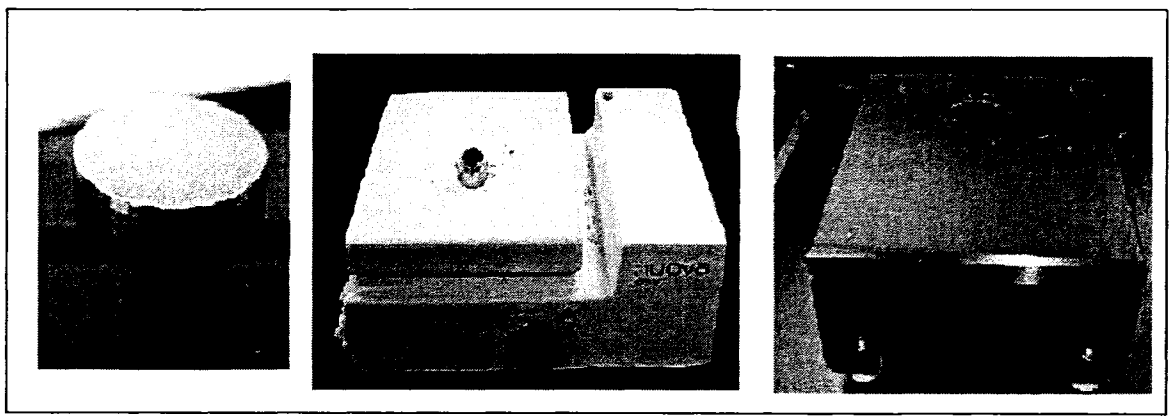

(a). Specimen Holder, Hot Plate and Flat plate

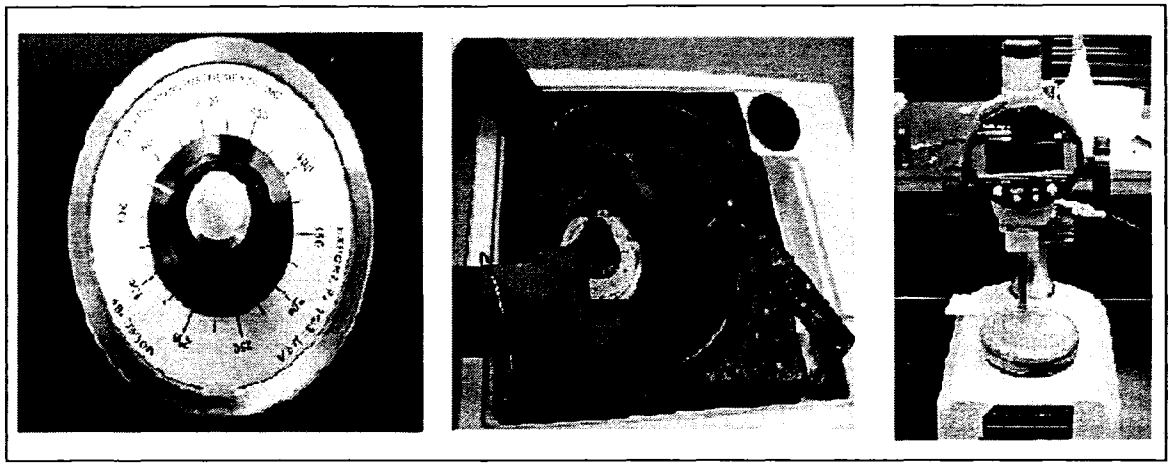

(b). Mechanical Polishing

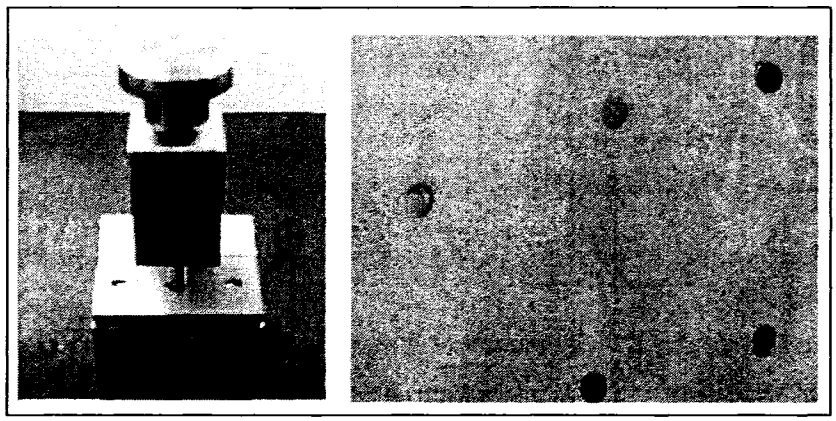

(c). Puncher and Specimen after Punching

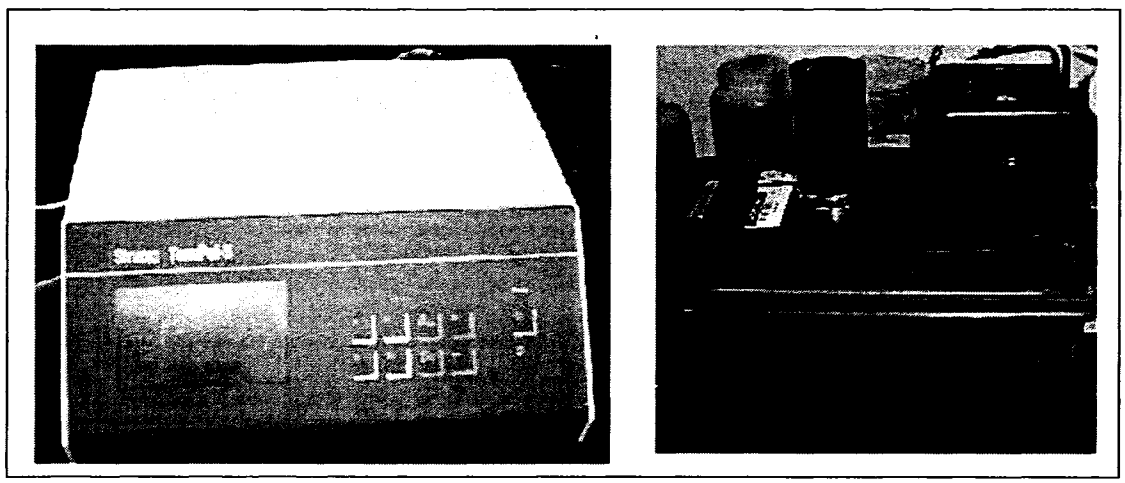

(d). Electrochemical Polishing Unit

Figure 3.2. TEM Specimen Preparation

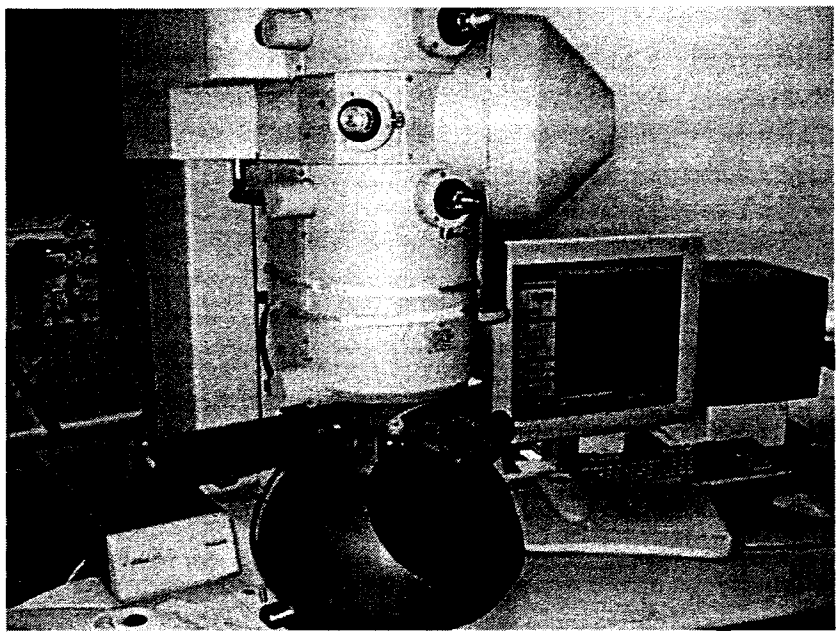

Figure 3.3. Transmission Electron Microscope

The magnitude of (ρ) for each specimen was determined by using a line-intersection method[13,14] through superimposition of a grid consisting of horizontal and vertical test lines on the resultant TEM micrographs that contained dislocations of different concentrations. A typical TEM micrograph of Nb7.5Ta tested specimen, showing dislocations and a grid of horizontal and vertical test lines, is illustrated in Figure 3.4. The total lengths of both the horizontal and vertical test lines of the superimposed grid was then measured. Eventually, the number of intersections of these test lines with dislocations was counted. The dislocation density was computed using Equation 3.5, given below.

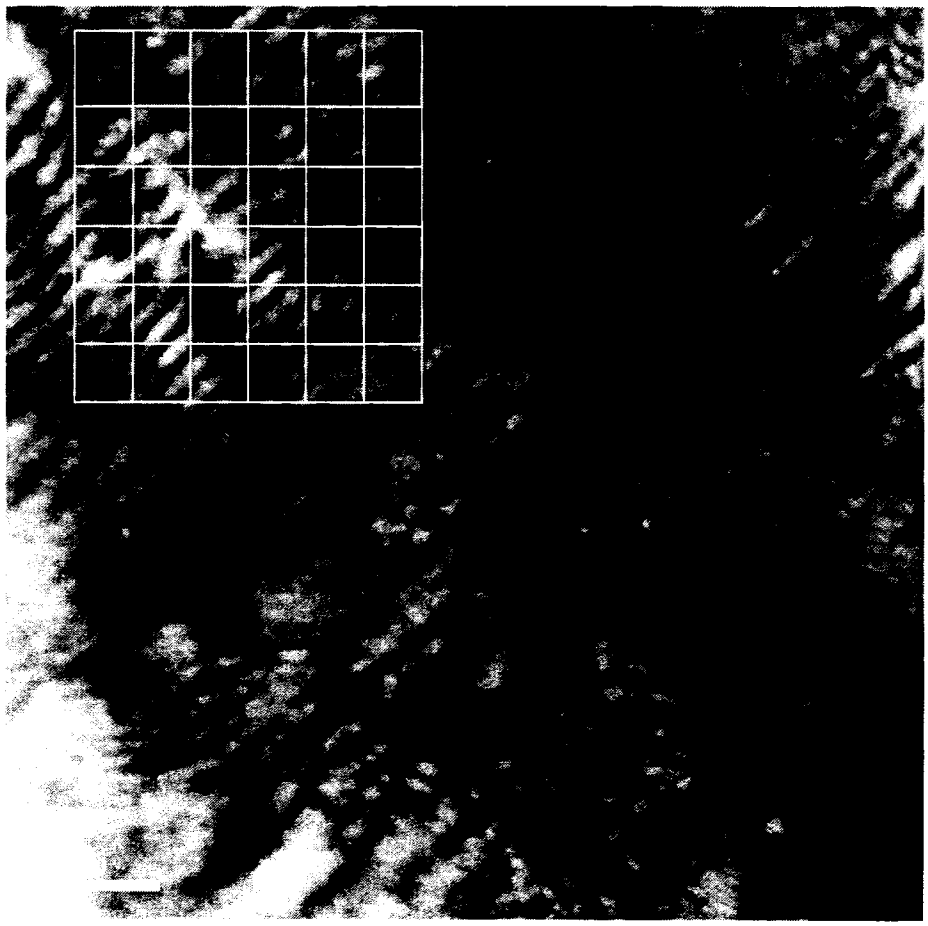

Figure 3.4. Line Intersection Method to Calculate Dislocation Density

$$\rho = \frac{1}{t}\left(\frac{\sum n_v}{\sum L_V} + \frac{\sum n_h}{\sum L_h}\right) \qquad \text{Equation (3.5)}$$

where,

Σn_v = No. of intersections of vertical test lines with dislocations

Σn_h = No. of intersections of horizontal test lines with dislocations

ΣL_h = Total length of horizontal test lines, meter (m)

ΣL_v = Total length of vertical test lines (m)

Efforts were made to calculate ρ at multiple locations of the resultant TEM micrograph of a specimen tested at each temperature (room temperature, 300 and 400°C). An average value of ρ was then computed based on the calculated values obtained at different locations of this micrograph. The thickness (t) of each specimen was measured using the electron-energy-loss-spectroscopic (EELS) [15] method available with the TEM. An average value of t based on the measurement of thickness at different locations of each specimen was determined by using Equation 3.6, as shown below.

$$t = \lambda \ln(I_T / I_O) \qquad \text{Equation (3.6)}$$

t = Average thickness of the sample

I_t = Total intensity reaching the spectrometer

I_o = Zero-loss intensity reaching the spectrometer

λ = Mean free path

3.3 Stress-Corrosion-Cracking Evaluation

3.3.1 Constant-Load Testing

SCC testing was performed using cylindrical specimens under a constant load. A calibrated proof ring, designed by Cortest Inc. to meet the National Association of Corrosion Engineers (NACE) standard TM-01-77 [16], was used to load these specimens at the desired levels. A calibration curve, showing load vs. deflection, was provided by this vendor for each proof ring. The amount of displacement needed to apply a desired load to the test specimen was determined from these calibration curves. A typical

calibration curve for the proof ring used in this investigation is shown in Figure 3.5. A dial gage was used to measure the magnitude of the desired displacement.

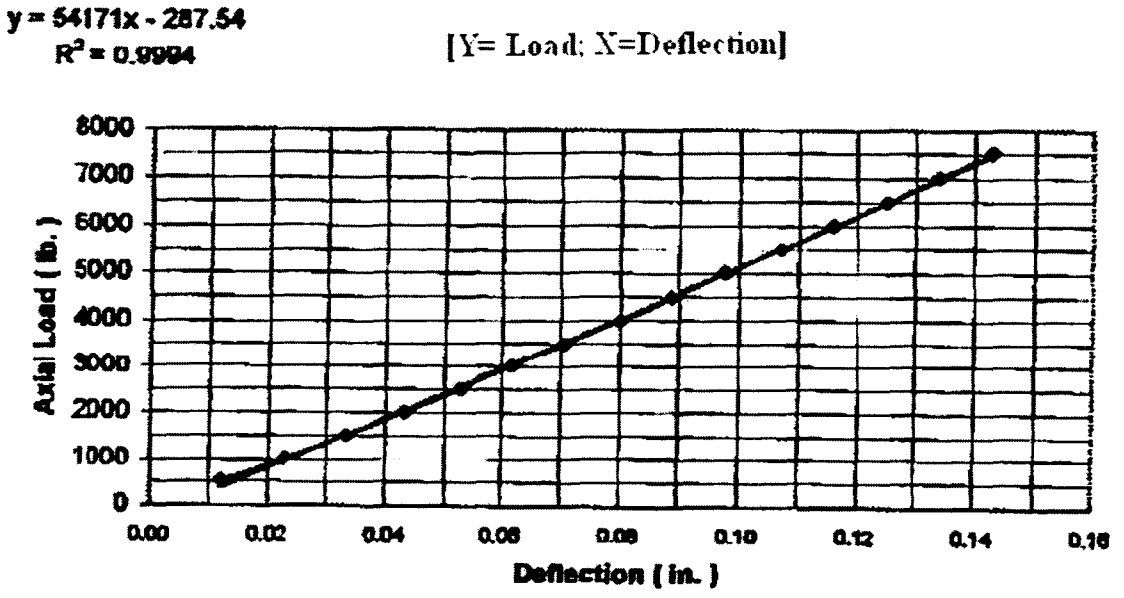

Figure 3.5. Proof Ring Calibration Curve

The SSC testing under a constant loading condition was performed using a metallic chamber made of highly corrosion resistant Alloy C-276 that contained the acidic solution. A pictorial view of the test cell is shown in Figure 3.6. Heating cartridges were inserted at the bottom cover of the test cell to apply the desired temperature to the solution contained inside the test vessel. This chamber was secured with O-ring seals to prevent leakage during testing. Condensers were used at the top cover of the loading chamber to prevent the liquid-loss due to the evaporation of solution when tested at the elevated temperatures.

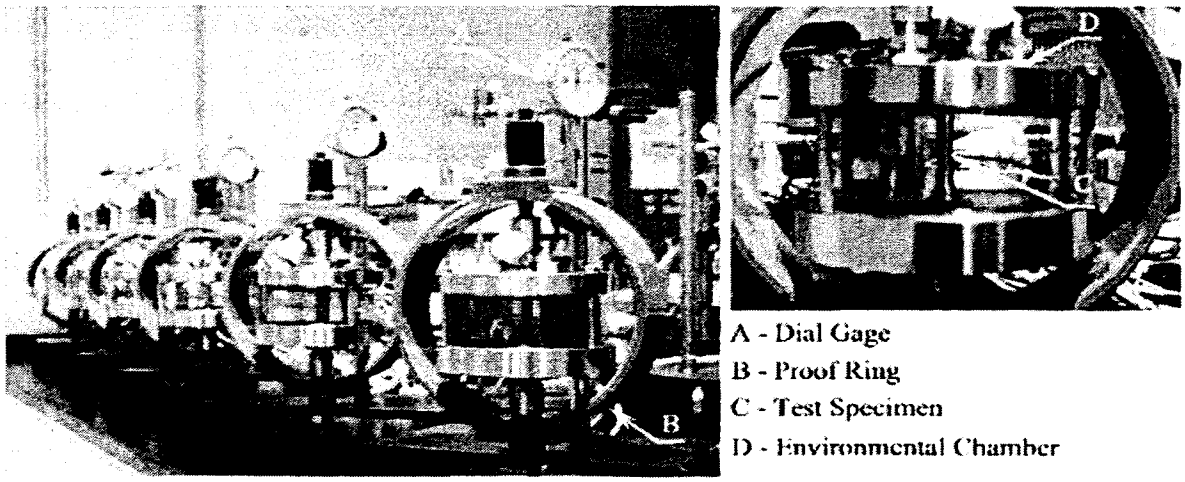

Figure 3.6. Constant-Load Test Setup

The magnitude of the stress applied to the cylindrical specimen was based on the ambient temperature tensile YS of Nb7.5Ta. The specimen was loaded at 98 % of its room temperature YS value and corresponding time-to-failure was automatically recorded using a timer attached to the top of this proof ring. The SCC testing was performed for a maximum duration of 30 days. The cracking susceptibility under a constant loading condition was expressed in terms of the TTF and a threshold stress (σ_{th}) below which no failure occurred within 30 days. If the test specimen survived the applied stress for 30 days, a threshold stress equivalent to that applied stress was reported.

3.3.2 Slow-Strain-Rate Testing

A specially-designed system, known as a constant-extension-rate-testing (CERT) device, was used to perform SCC testing under a SSR condition. The test specimen was pulled at a constant strain rate according to the ASTM Designation G 129 [17]. The CERT machine enabled an evaluation of the cracking tendency of the test material simulating a

broad range of load, temperature, strain-rate and environmental conditions. This machine was capable of providing a maximum load of 7500 lbs to the specimen with linear extension rates ranging from 10^{-5} to 10^{-8} in/sec during straining.

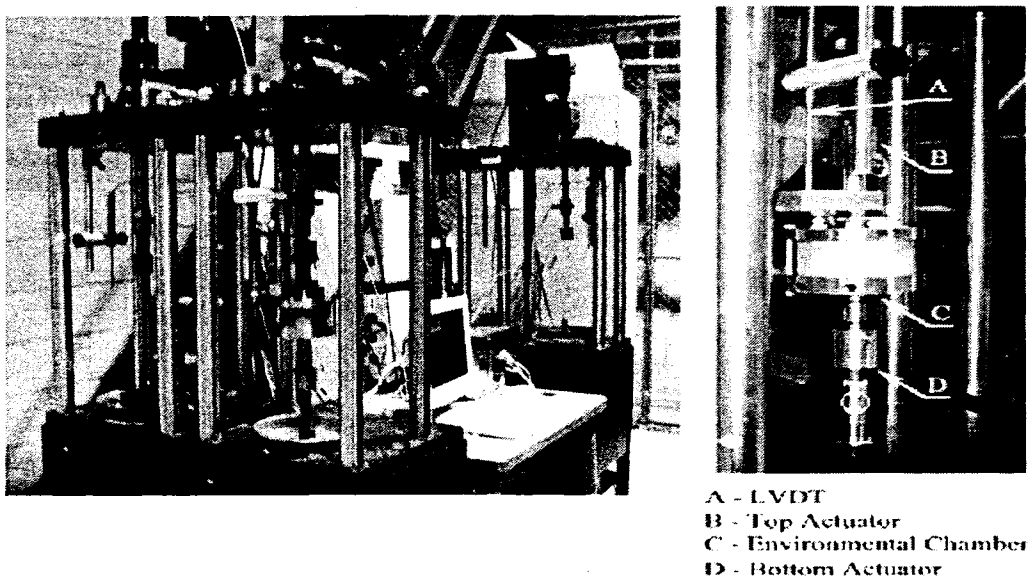

Figure 3.7. CERT Machine for SCC Testing

The SSR test setup used in this investigation consisted of a top-loaded actuator, testing chamber, linear-variable-differential-transducer (LVDT) and a load cell, as shown in Figure 3.7. The specimens were pulled at a preferred strain rate using a top-loaded actuator to prevent any damage resulting from the spilled test solution. As in the case of constant-load testing, heating cartridges were connected to the bottom cover of the environmental chamber for elevated-temperature testing. A thermocouple was connected through the top cover of this chamber to monitor the testing temperature. The load cell

measured the applied load, and the extension of the test specimen due to straining was monitored by the LVDT.

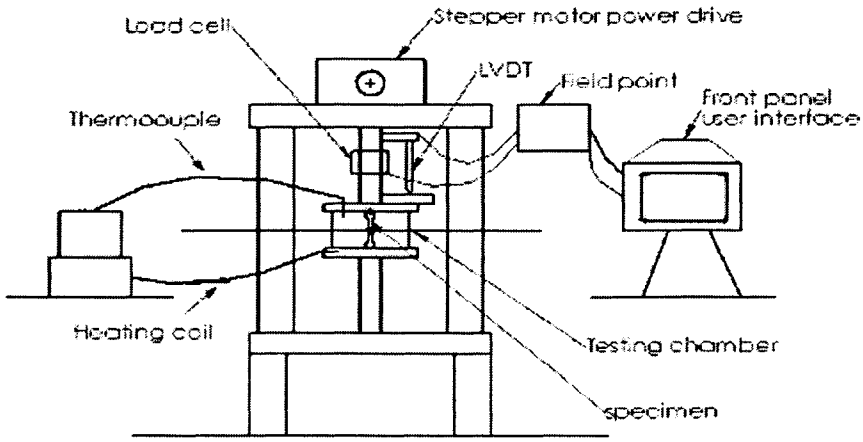

Figure 3.8. SSR Test Setup

The occurrence of SCC in susceptible metals and alloys is the result of synergistic effect of applied or residual stress and a hostile environment. If the stress is applied to a specimen at a very fast rate, similar to that of the conventional tensile testing, the resultant failure could simply represent mechanical deformation even in the presence of an environment. On the contrary, if the applied strain rate is too slow, the resultant damage is primarily due to the breakdown of the protective surface films from prolonged interaction of the test material with the potent environment.

Thus, in order to evaluate the cracking susceptibility of a material of interest in an environment using the SSR technique, it is customary to apply an optimum strain rate that can provide a maximum contribution of both the strain rate and the environment to

promote embrittlement in the presence of a susceptible environment. In view of this rationale, a strain rate of 3.3×10^{-6} sec^{-1} was applied to the specimen during SCC testing under the SSR condition. The selection of the strain rate was based on prior testing experience at the Lawrence Livermore National Laboratory (LLNL) [18-20]. The application of this strain rate ensured the failure of the cylindrical specimens due to the synergistic effect of applied load and the acidic solution used in this investigation.

The SSR testing data were expressed in terms of engineering stress vs. strain (s-e) diagrams. Dimension (length and diameter) of the test specimen was measured before and after testing. The cracking tendency of the test specimen under this condition was determined by the time-to-failure, and a number of ductility parameters including %El and %RA. Further, the true failure stress (σ_f) determined from the s-e diagram and the final specimen dimension was used to characterize the cracking tendency of the test material. The magnitudes of %El, %RA and σ_f based on duplicate testing were determined by using the following equations:

$$\%\,\mathrm{El} = \left(\frac{L_f - L_o}{L_o}\right)\times 100 \qquad \text{(Equation 3.7)}$$

$$\%\mathrm{RA} = \left(\frac{A_o - A_f}{A_o}\right)\times 100 \qquad \text{(Equation 3.8)}$$

$$\sigma_f = \frac{P_f}{A_f} \qquad \text{(Equation 3.9)}$$

$$A_o = \frac{\pi \times D_o^{\,2}}{4} \qquad \text{(Equation 3.10)}$$

$$A_f = \frac{\pi \times D_f^{\,2}}{4} \qquad \text{(Equation 3.11)}$$

Where,

A_0 = Initial cross sectional area

A_f = Cross sectional area at failure

P_f = Failure load

σ_f = True Failure Stress

L_o = Total initial length

L_f = Total final length

D_o = Initial gage diameter

D_f = Final gage diameter

3.4 Cyclic Potentiodynamic Polarization Testing

The structural materials may become susceptible to degradations when subjected to an aggressive electrolyte such as an acidic solution due to the influence of electrochemical factors. Pitting and crevice corrosion are two classical examples of this type of attack. Polarization methods such as potentiodynamic and potentiostatic polarization are often used to characterize localized corrosion of engineering metals and alloys. These techniques can provide useful information on the corrosion mechanisms, the corrosion rate and the susceptibility of a specific material to corrosion in designated environments. Potentiodynamic polarization involves the application of an electrochemical potential at a specific rate, and monitoring the resultant changes in current.

This type of polarization can be divided into two types, namely anodic and cathodic. During anodic polarization of a metal, an external potential is applied to the specimen in the anodic (positive) direction causing it to undergo dissolution by forming metallic ions and generating electrons that can be used during cathodic (negative) reaction. The cyclic potentiodynamic polarization (CPP) method used in this investigation consisted of initial cathodic polarization followed by an anodic potential scan. The CPP technique is capable of identifying the different types of critical potentials, namely corrosion or open circuit potential (E_{corr}), critical pitting potential (E_{pitt}), and protection potential (E_{prot}), if any.

A Gamry potentiostat [21] (model PC14) was used to perform CPP experiments involving cylindrical specimens of Nb7.5Ta. Prior to the CPP testing, this potentiostat was calibrated according to the ASTM Designation G 05 [22]. Such calibration uses a Type 430 ferritic stainless steel exposed to a 1N H_2SO_4 solution at 30°C, and anodically polarizing it at a potential scan rate of 0.17 mV/sec. A typical polarization curve obtained from the calibration experiment is illustrated in Figure 3.9. If the generated calibration curve matches with the typical anodic polarization diagram shown in the ASTM G5 Standard, the equipment is construed to be performing accurately.

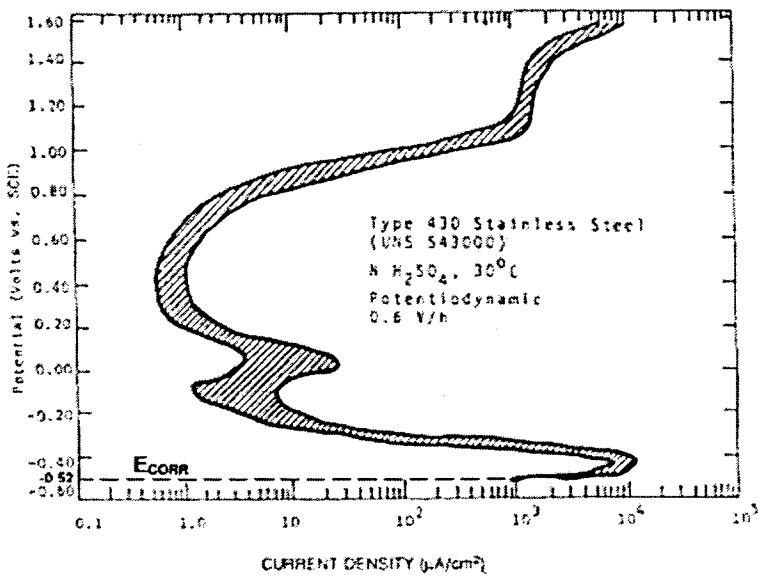

Figure 3.9. ASTM G 05 Standard Calibration Curve

A three electrode polarization technique was used to evaluate the localized corrosion susceptibility of Nb7.5Ta using the calibrated Gamry potentiostat. The test specimen was used as a working electrode, two graphite rods were used as counter electrodes and silver/ silver chloride (Ag /AgCl) solution contained in a Lugin probe acted as the reference electrode. The CPP test setup used in this study is illustrated in Figure 3.10. The tip of the Lugin probe was placed within two to three mm of the working electrode. The test solution contained inside the polarization cell was de-aerated by bubbling N_2 through it for 45 minutes. Prior to the polarization experiment, an initial delay of 30 minutes was given to the specimen contained in the test solution to achieve a stable E_{corr} value. Subsequently, a potential was applied to the specimen at a rate of 0.17 mV/sec in the forward direction. The magnitude of E_{pit}, if any, was determined from the change in slope during transition from a passive region to a transpassive region. The potential (E) was then reversed, and the resultant changes in current (I) were plotted as E vs. logI. Such

potential scan with many materials can show a positive hysteresis loop, identifying E_{prot}, if any, by the intersection of this loop with the passive region of the CPP diagram.

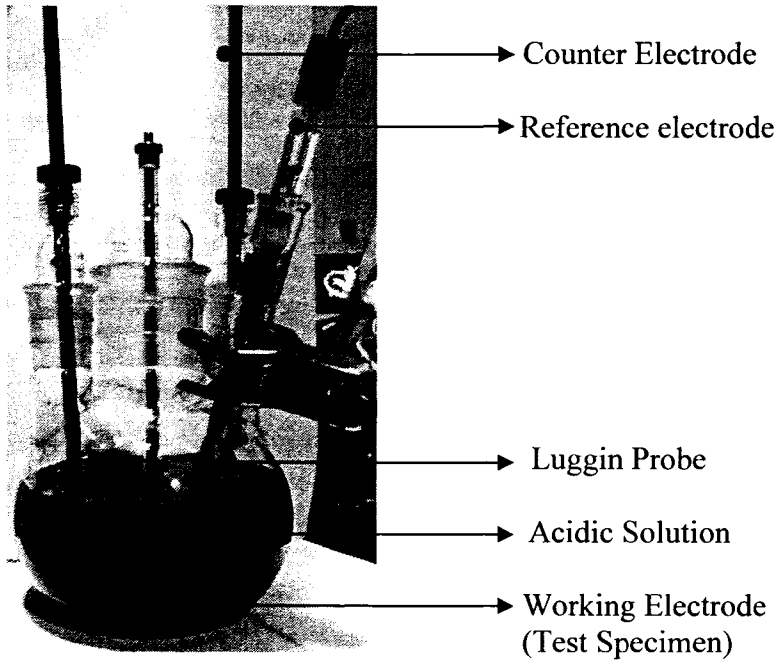

Figure 3.10. CPP Test Setup

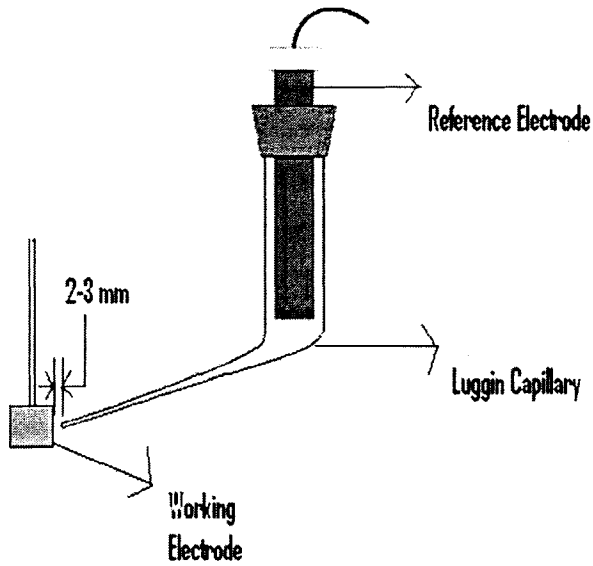

Figure 3.11. Luggin Probe Arrangement

3.5 SCC Testing under Potentiostatic Control

As indicated earlier, H_2 will be generated by the decomposition of the HI_x process using the S-I cycle. Therefore, an effort was made to evaluate the cracking susceptibility of Nb7.5Ta under the influence of H_2 generated from the acidic solution. It is well known that during cathodic polarization the hydrogen ion (H^+) can be reduced into an atomic hydrogen (H) resulting from its combination with an electron generated during the anodic reaction. The amount of H generated from cathodic reaction increases with more active (negative) potential. These atomic hydrogen can eventually combine to form molecular hydrogen (H_2). Thus, in order to study the effect of H_2 on the cracking susceptibility of Nb7.5Ta, cathodic potentiostatic polarization experiment was performed using a cathodic applied potential (E_{cont}) in an identical environment. The magnitude of E_{cont} was based on the measured E_{corr} value in the same environment according to the equation shown below.

$$\eta = E_{cont} - E_{corr} \qquad \text{(Equation 3.12)}$$

where η = Overvoltage

E_{cont} = Controlled potential

E_{corr} = Corrosion potential

Smooth cylindrical specimens were used for SCC testing under E_{cont}. In order to apply the external potential from the calibrated potentiostat, the top shoulder of the cylindrical specimen was spot-welded with a conductive metallic wire to allow electron flow to the central portion of the gage section during straining under the SSR condition. Prior to the application of E_{cont}, the conductive wire was coated with a lacquer to prevent its direct contact with the test solution during straining. The selected E_{cont} value was then applied to the test specimen for the entire straining period until it failed. The cracking susceptibility under cathodic E_{cont} was expressed in terms of the ductility parameters (%El and %RA), TTF and σ_f. A pictorial view of the spot-welded cylindrical specimen and the experimental setup used in the E_{cont} testing are illustrated in Figures 3.12.

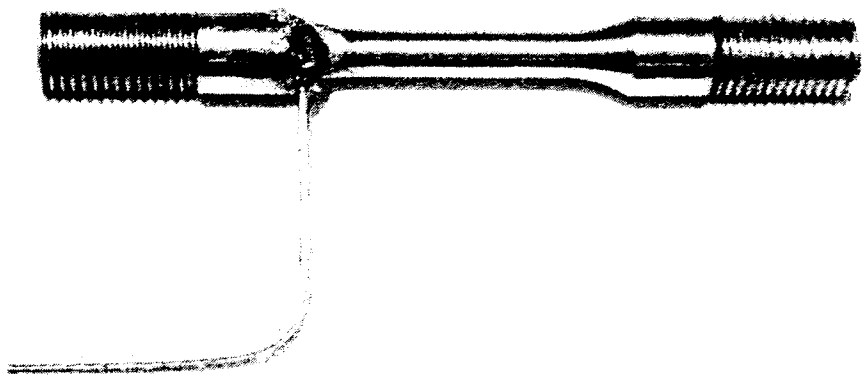

(a). Spot-welded Cylindrical Specimen

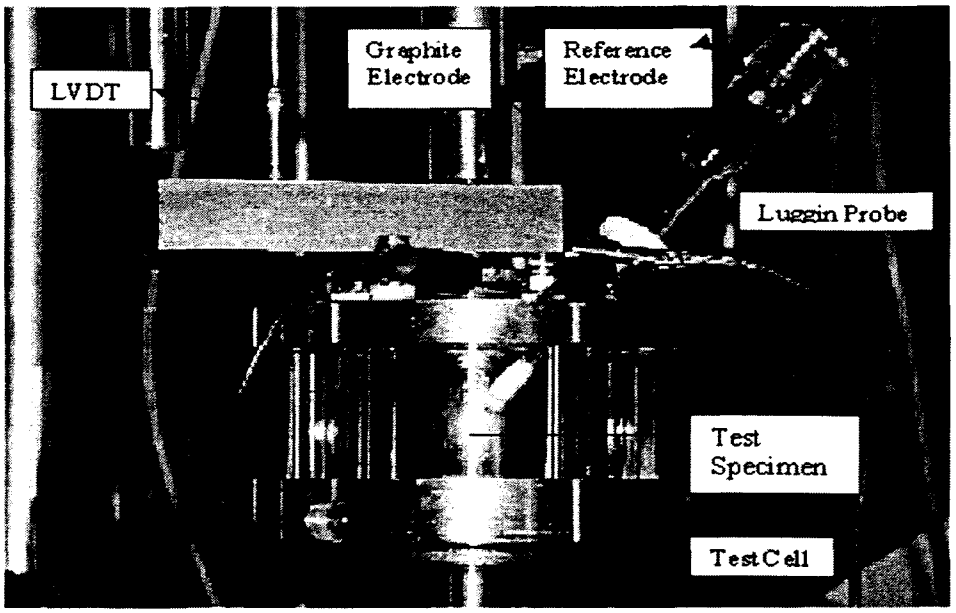

(b) Test Setup

Figure 3.12. Applied Potential Test Setup

3.6 Metallographic Evaluation

A Leica inverted Optical Microscope, shown in Figure 3.13, with a maximum resolution of 1000X [23] was used to characterize the metallurgical microstructures of the tested material. The optical microscopic evaluation is based on the impingement of high energy light rays onto the specimen surface, and transmitting them through a number of condensing lenses and shutters into a half-penetrating mirror. The transmitted light then passes through an objective lens forming a primary image, which is magnified through the eyepiece. A digital camera with a resolution of 1 mega pixel and a software interface enabled the development of the microstructures on a computer screen. A section of the as-received material (Nb7.5Ta) was mounted in an epoxy resin. The mounted specimen

was then subjected to polishing and etching according to the standard metallographic procedures using Buehler polishing wheels. The etchant used was a solution of hydrofluoric acid (HF), nitric acid (HNO_3) and glycerol, the volumetric composition of which is given in Table 3.2.

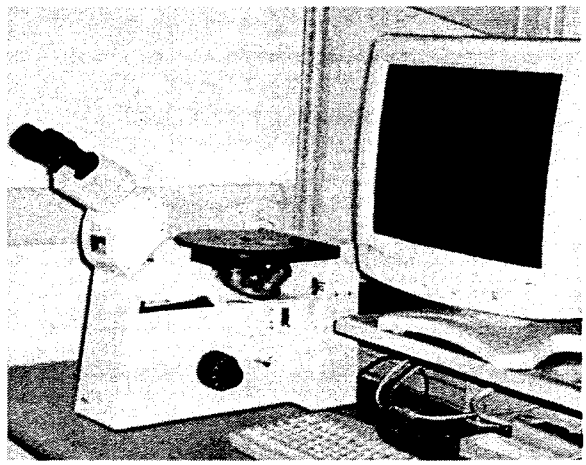

Figure 3.13. Optical Microscope

Table 3.2. Volumetric Composition of the Etchant

HF	HNO_3	Glycerol	Etching time, sec
60%	20%	20%	10sec

3.7 Fractrographic Evaluation

Fractrographic evaluation by SEM enabled the determination of the extent and morphology of failure at the primary fracture surface of the tensile specimens tested at different temperatures. The characteristics of failure such as ductile vs. brittle and intergranular vs. transgranular can be determined from such fractrographic evaluations. A

JEOL SEM (Model no – 5610) having a maximum magnification of 100,000X was used to analyze the fracture characteristics of the tested specimens. This SEM was equipped with secondary and back scattered electron detectors, an Oxford ISIS energy dispersive spectroscopic (EDS) system. The EDS was capable of analyzing elements present in the vicinity of the fracture surface. The SEM unit used in this investigation is shown in Figure 3.14

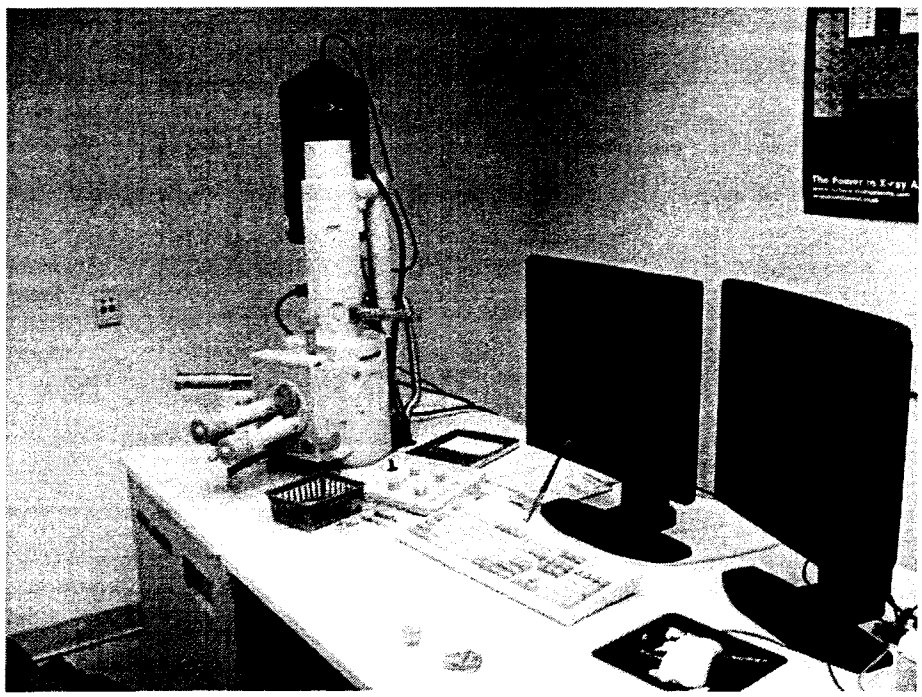

Figure 3.14. SEM Setup

CHAPTER 4

RESULTS

This chapter presents the results of tensile testing and corrosion studies involving Nb7.5Ta, which is a candidate refractory material proposed to be used in hydrogen generation resulting from the decomposition of HI_x. The tensile data have been presented in terms of different mechanical parameters as a function of temperature. The results of stress corrosion cracking (SCC) and localized corrosion studies have also been included in this chapter. In addition, metallographic and fractrographic evaluations using conventional analytical techniques are presented. The test results corresponding to individual type of testing are discussed next in the following subsections.

4.1 Metallographic Evaluation

The optical micrographs of Nb7.5Ta obtained in an etched condition is illustrated in Figure 4.1. An examination of this micrograph reveals the presence of equiaxed grains consisting of niobium (Nb) and tantalum (Ta). While, the dark grains represent Ta, the white grains correspond to Nb, as cited in the literature [24].

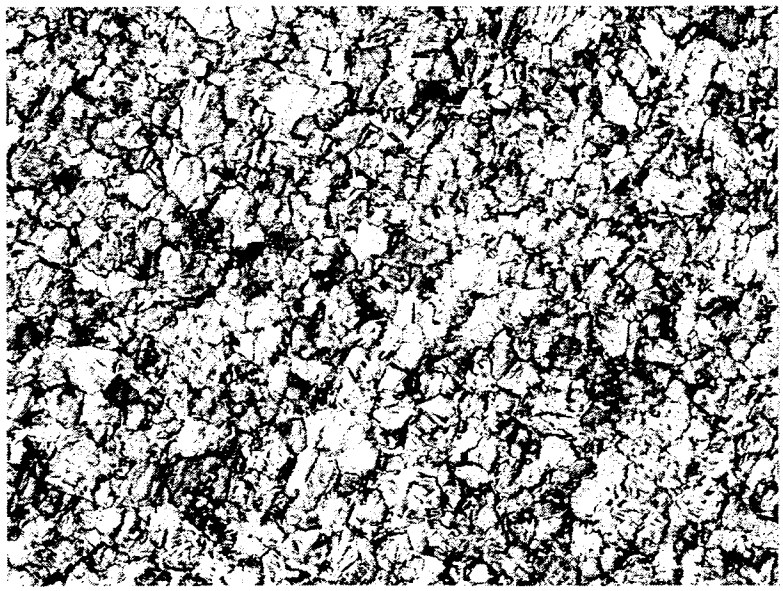

Figure 4.1. Optical Micrograph, HF + HNO_3 + Glycerol, 100X

4.2 Tensile Properties Evaluation

The results of tensile testing using smooth cylindrical specimens of Nb7.5Ta are illustrated in Figure 4.2 in a superimposed manner in the form of engineering stress vs. strain (s-e) diagram as a function of the testing temperature. Testing was performed at room temperature, 100, 200, 300 and 400°C. A temperature of 400°C has been proposed to be the maximum operating temperature for decomposition of HI_x. An evaluation of these s-e diagrams indicates that the magnitude of the yield strength (YS) and the ultimate tensile strength (UTS) was gradually reduced with increasing temperature due to ease of plastic deformation at elevated temperatures. However, an interesting observation was noted in that, the magnitude of the failure strain (e_f) was gradually reduced with an increase in temperature within a temperature regime of ambient to 300°C. Beyond 300°C, the magnitude of e_f was increased, indicating enhanced ductility. The observed phenomenon of reduced ductility in terms of e_f within a specific temperature regime has

been termed as dynamic strain aging (DSA) of metallic materials and alloys. The DSA of engineering materials has been attributed to reduced plastic flow resulting from the pinning of dislocations at the grain boundaries.

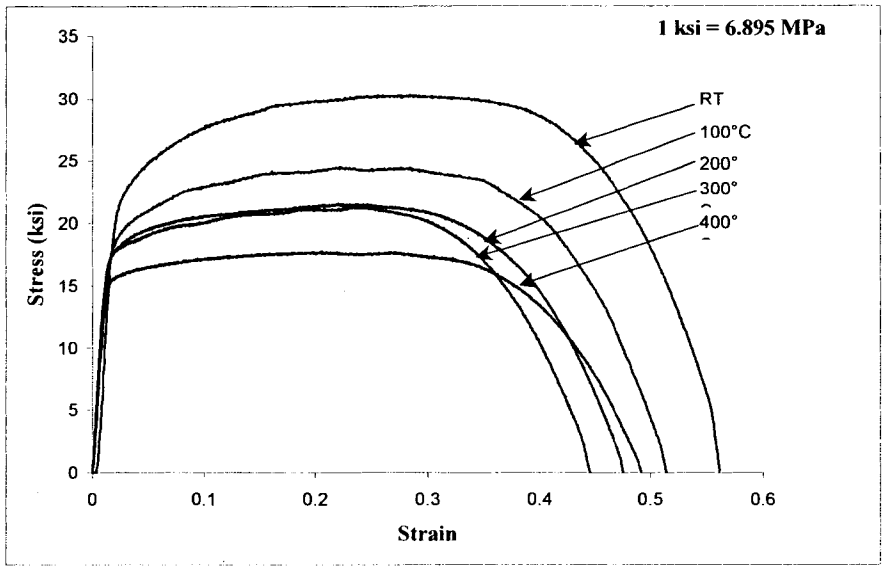

Figure 4.2. s-e Diagram vs. Temperature

The magnitudes of different tensile parameters that include YS, UTS, percent elongation (% El), and percent reduction in area (% RA) have been determined from the s-e diagrams and the specimen dimensions before and after testing as a function of the testing temperature. Table 4.1 shows the tensile properties of Nb7.5Ta at different temperatures. The data shown in this table are reproduced in Figures 4.3 through 4.6, showing the variation of all four parameters with temperature. A gradual drop in tensile strength was seen with increasing temperature, as illustrated in Figures 4.3 and 4.4. With respect to the ductility of Nb7.5Ta in terms of its % El, a gradual drop was seen in the

temperature range of ambient to 300°C. However, it should be noted that during duplicate testing, the magnitude of %El was almost similar at temperatures of 200 and 300°C, as presented in the Appendix. As to the %RA, its value was almost uniform, showing no significant variation with increasing temperature. A precise measurement of the cross-sectional area of the specimen upon completion of testing was extremely difficult due to the formation of very fine tips at the primary fracture surfaces of the broken cylindrical specimen.

Table 4.1. Tensile Properties at Different Temperatures

Temperature (°C)	YS, Ksi (MPa)	UTS, Ksi (MPa)	%El	%RA
RT	21.82 (150.48)	30.40 (209.60)	55.97	96.90
100	18.75 (129.28)	24.61 (169.67)	52.22	96.67
200	17.23 (118.77)	21.16 (145.90)	48.4	96.77
300	16.69 (115.07)	20.03 (140)	44.75	95.84
400	15.5 (106.87)	17.87 (122.73)	50.64	96.24

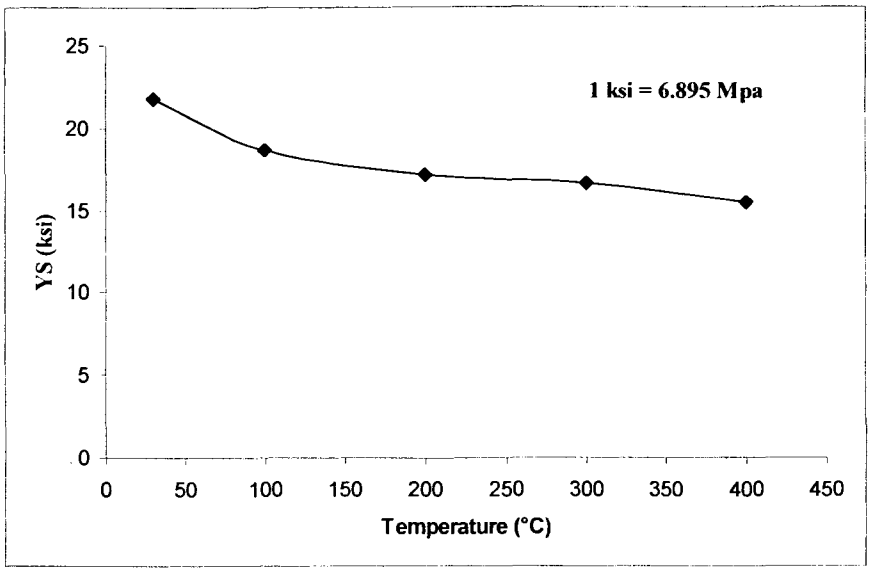

Figure 4.3. YS vs. Temperature

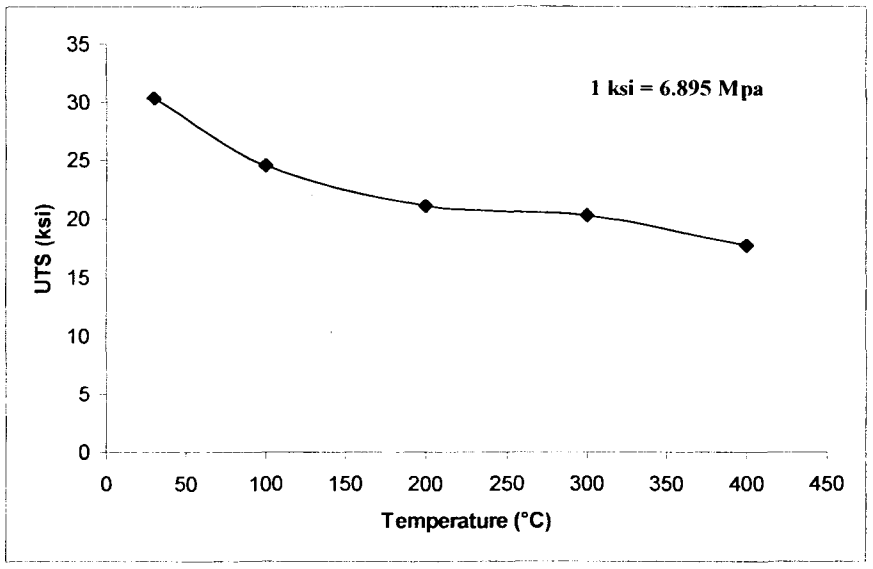

Figure 4.4. UTS vs. Temperature

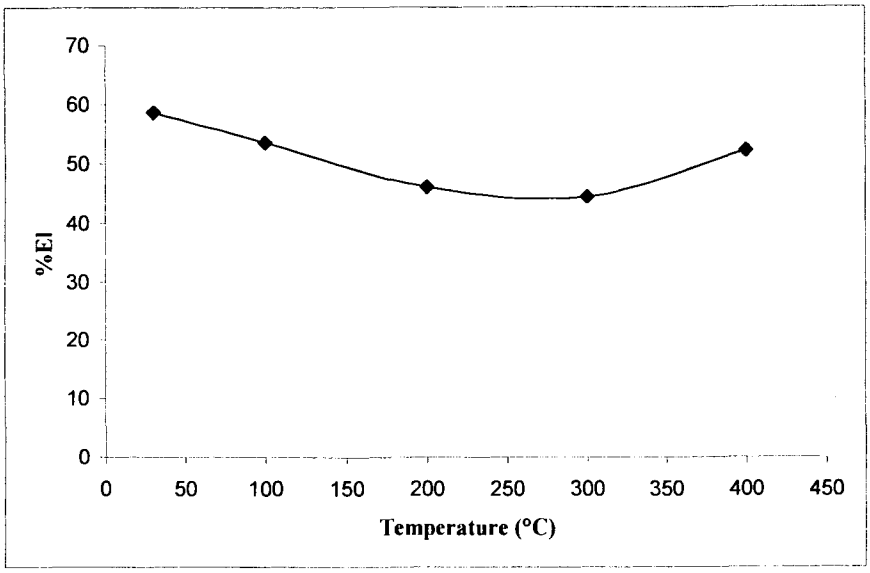

Figure 4.5. %El vs. Temperature

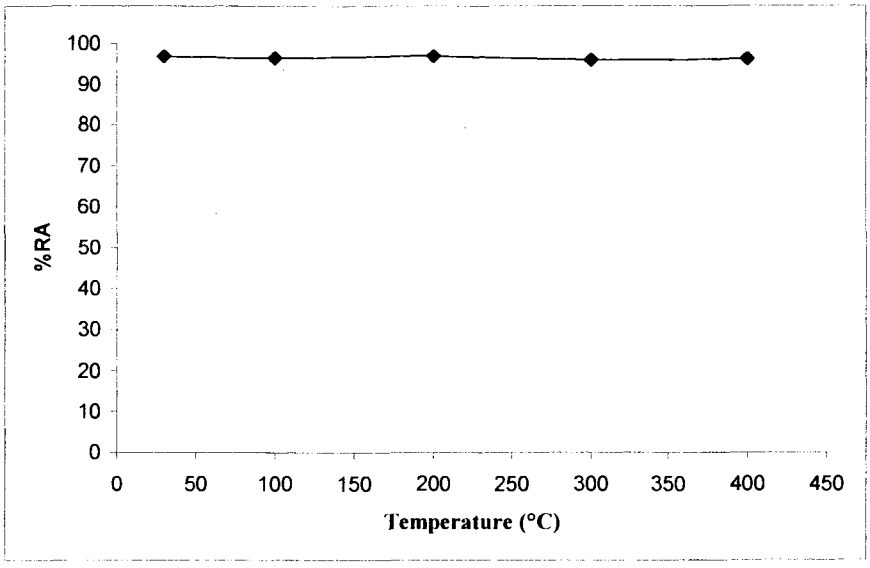

Figure 4.6. %RA vs. Temperature

As indicated earlier in this chapter, the gradually reduced e_f or % El values within a susceptible temperature regime are the result of DSA, which occurs due to the reduction in dislocation mobility within the grains and through the grain boundaries. The phenomenon of DSA is cited [8] to be the result of solute diffusion into the metal lattice, thus inhibiting the movement of dislocations past the grain boundaries. As a result of this reduced dislocation mobility, clusters of dislocations can be formed inside the metal lattice that can only be detected by transmission electron microscopy (TEM). In view of this rationale, significant effort has been made in this investigation to determine the dislocation density (ρ) of the specimens, tested at room temperature, 300 and 400°C using TEM. TEM analysis at room temperature was aimed at developing a baseline information with respect to the concentration of dislocations in terms of ρ. The specimens tested at temperature of 300 and 400°C were selected for TEM analyses to differentiate the concentration of dislocations at and above the susceptible temperature regime for the occurrence of DSA.

4.3 Characterization of Dislocations

TEM micrographs obtained on cylindrical specimens tested at room temperature, 300 and 400°C are illustrated in Figures 4.7. A cursory examination of these micrographs reveals that the concentration of dislocations in the specimen tested at 300°C was maximum compared to those of the specimens tested at room temperature and 400°C. It is interesting to note at this point that the extent of e_f was minimum in the temperature range of 200 to 300°C. Thus, the micrographs, shown in Figure 4.7, clearly verify the observation made from the s-e diagrams with respect to the ductility in terms of e_f. The

magnitudes of ρ, determined from these TEM micrographs by superimposition of grids as discussed earlier, are given in Table 4.2. It should be noted that the magnitude of the average ρ value at each temperature was based on the multiple ρ values determined from placement of the grid at 4 different locations of the TEM micrographs. An evaluation of the data, shown in Table 4.2, clearly indicates that the average value of ρ at 300°C was slightly higher compared to that at 400°C. The relatively lower ρ value in the specimen tested at 400°C signifies somewhat reduction in dislocation concentration due to increased dislocation mobility, as evidenced by greater e_f value in the s-e diagram. At room temperature, the ρ value was one order magnitude lower compared to that at 300 and 400°C, suggesting thinner dislocation clusters and reduced solute diffusion through the metal lattice.

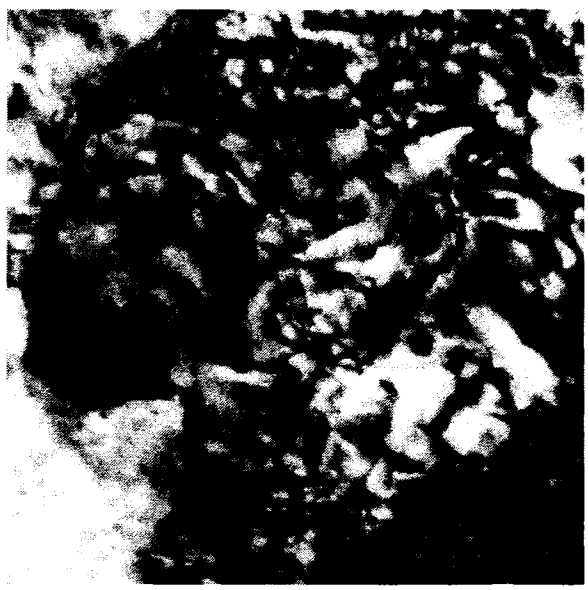

(a) Room Temperature, 120K Magnification

(c) 300°C, 250K Magnification

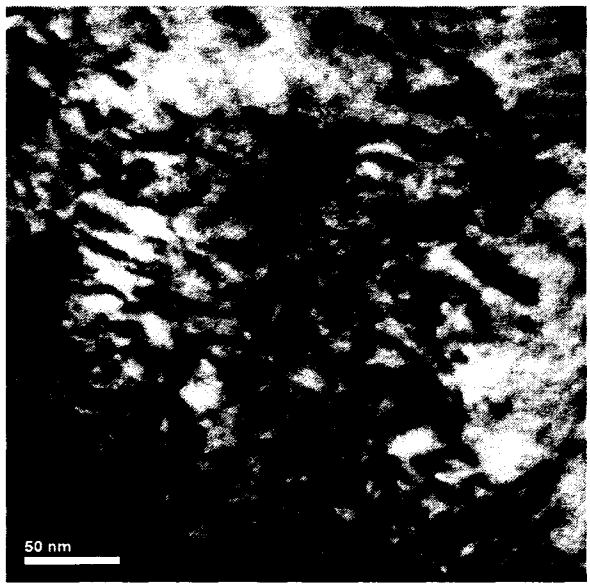

(d) 400°C, 120K Magnification

Figure 4.7. TEM Micrographs of Tensile Specimens Tested at Different Temperatures

Table 4.2. Dislocation Density at Different Temperatures

Test temperature, °C	Dislocation Density (ρ), No./m^2
Room Temperature	3.45×10^{13}
300	2.49×10^{14}
400	2.34×10^{14}

4.4 SCC Evaluation

The results of stress corrosion cracking (SCC) testing in an acidic solution involving Nb7.5Ta indicate that this alloy did not exhibit any cracking susceptibility at room temperature and 90°C under a constant loading condition. This material was immune to SCC even under an applied stress equivalent to 98% of its room temperature YS value. The results of SCC testing in an identical environment using the SSR technique are illustrated in Figure 4.8, showing the cracking susceptibility of Nb7.5Ta in the form of s-e diagram as a function of the testing temperature. This figure also exhibit the effect of two different environments namely, air and acidic solution on the cracking tendency of this alloy. An evaluation of these data indicates that the nature of the s-e diagram did not change at room temperature despite the use of an acidic solution. These data may suggest that Nb7.5Ta may not exhibit any detrimental effect as to the cracking susceptibility in the presence of an acidic solution at ambient temperature. However, a significant difference in the s-e diagram was observed at 90°C in the presence of the acidic solution, showing reduced values of YS, UTS, e_f and the true failure stress (σ_f). Usually, the cracking susceptibility of a material in a susceptible environment under a SSR condition is expressed in terms of σ_f, TTF, %El and %RA. However, the determination of %RA

was extremely difficult in this study for a ductile material such as Nb7.5Ta since the final cross-sectional area of the test specimen could not be determined due to the formation of fine tips at the fracture surface.

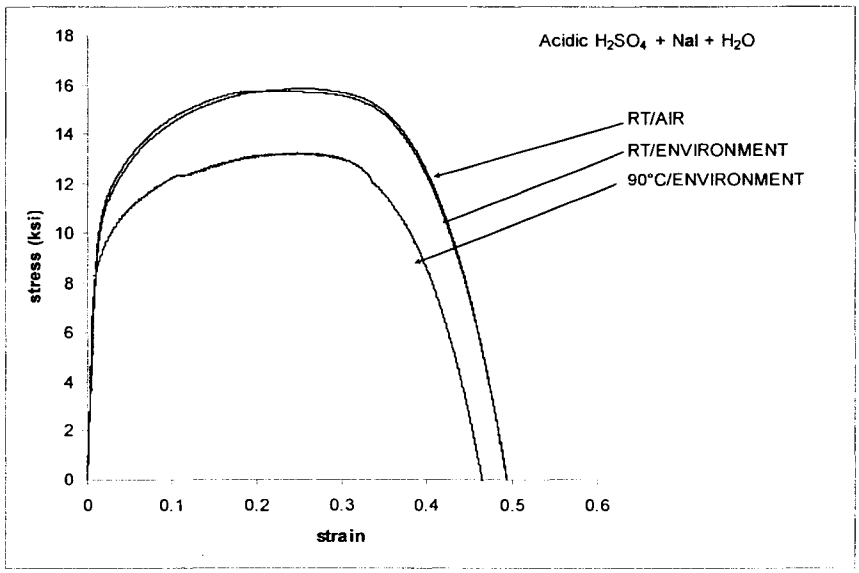

Figure 4.8. Comparison of s-e diagram in SSR Testing

The magnitudes of different parameters (%El, σ_f, TTF) obtained from the s-e diagrams and the dimensions of the specimens before and after testing are illustrated in Table 4.3. An evaluation of the overall SSR testing data, shown in this table, indicates that the cracking susceptibility was more pronounced in the 90°C acidic solution, showing the lowest values of all three parameters.

Table 4.3. SSR Test Results

Environment/ Specimen Type	Temperature, °C	%El	σ_f, ksi (MPa)	TTF, hours
Air/Smooth Tensile	RT	52.86	334.46 (2306)	43.54
Acidic Sol. /Smooth Tensile	RT	53.78	329.36 (2271)	43.70
Acidic Sol. /Smooth Tensile	90	50.34	290.59(2003)	40.49

4.5 Localized Corrosion Evaluation

The susceptibility of Nb7.5Ta to localized corrosion was studied by using the cyclic potentiodynamic polarization (CPP) technique in a 30°C acidic solution. A typical polarization diagram is illustrated in Figure 4.9 showing the magnitude of the corrosion potential (E_{corr}) and the critical pitting potential (E_{pit}). The determination of the protective potential (E_{prot}) could not be accomplished due to the formation of a negative hysteresis loop during reverse potential scan. The formation of a negative hysteresis loop signifies the formation of fresh oxide films resulting from the formation of oxygen due to electrolysis at high current, and its combination with Nb and Ta. No attempt has been made in this study to analyze the composition of these surface films. The localized corrosion susceptibility at elevated temperatures could not be determined due to the malfunctioning of the potentiostats.

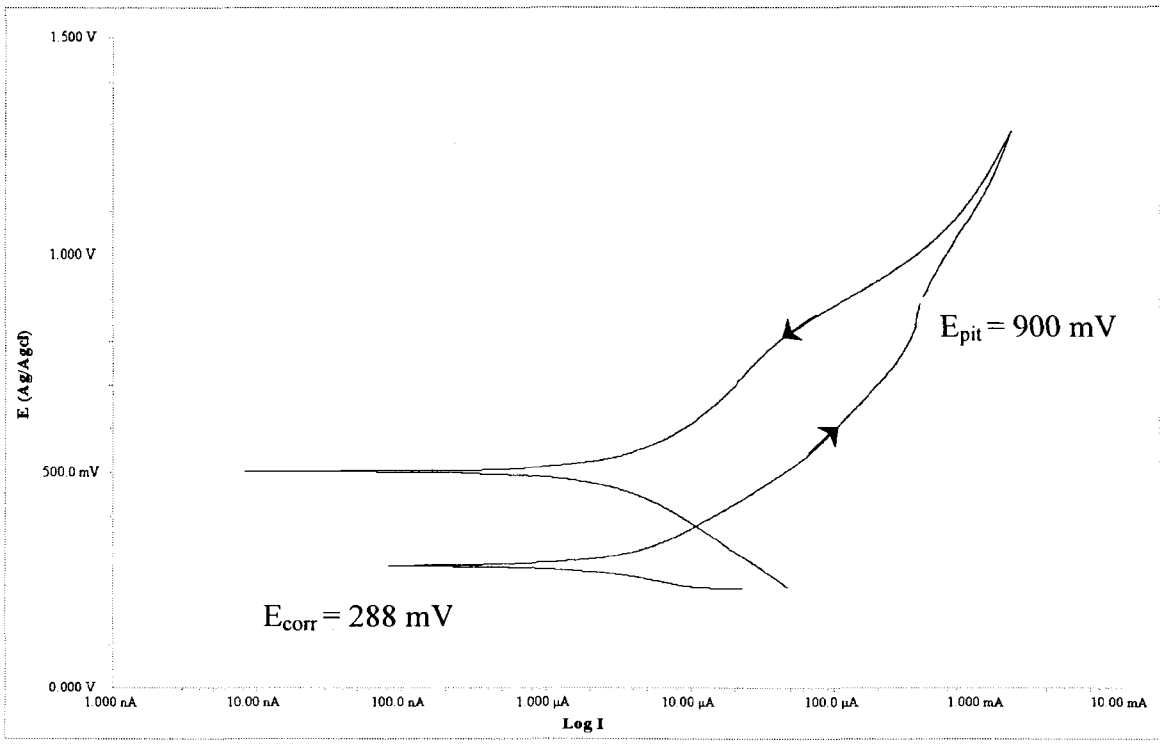

Figure 4.9. CPP Diagram at 30°C

4.6 SCC Testing under Cathodic Controlled Potential

As discussed earlier in this thesis, the refractory material such as Nb7.5Ta may undergo reaction with HI_x leading to the occurrence of hydrogen-induced damage, also known as hydrogen embrittlement (HE). In order to simulate the effect of atomic hydrogen (H) on the cracking susceptibility of this alloy, SCC testing was performed under a cathodic potentiostatic (constant potential) control using the SSR technique. The magnitude of this controlled potential (E_{cont}) was based on the E_{corr} value obtained from the CPP testing in an identical environment at room temperature. An E_{cont} value corresponding to -100 mV (Ag/Agl) of over voltage (η) was used during this potentiostatic experiment. The magnitude of E_{cont} based on this η value was +220 mV

(Ag/AgCl). The s-e diagrams obtained during SSR testing involving cylindrical specimen of Nb7.5Ta, with and without the application of E_{cont} are superimposed for comparative analysis, as illustrated in Figure 4.10. An examination of these s-e diagrams indicates that the magnitude of e_f was reduced when an external potential of 220 mV (Ag/AgCl) was applied to the cylindrical specimen during straining in an acidic solution at ambient temperature. This data suggest that Nb7.5Ta may become susceptible to HE during the HI_x decomposition process that will produce hydrogen, thus shifting the potential to more negative values.

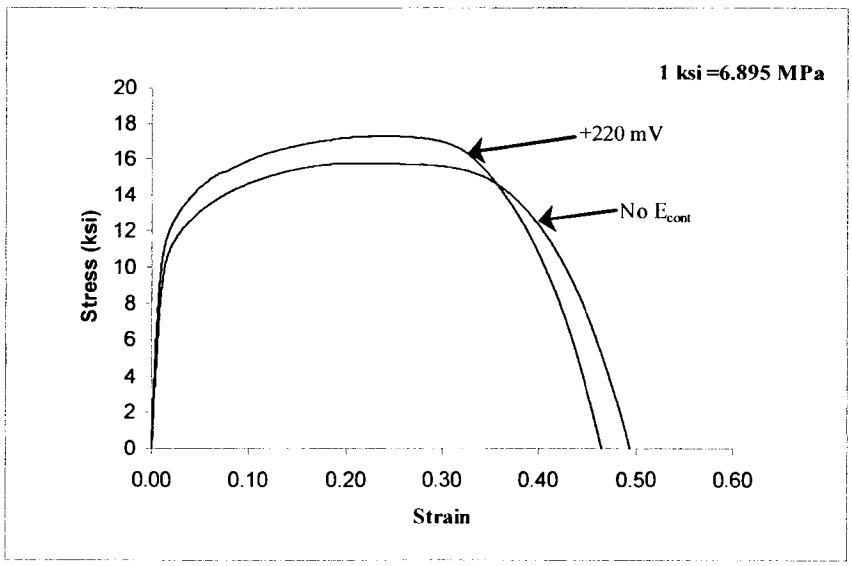

Figure 4.10. s-e Diagrams, with and without E_{cont}

4.7 Fractrographic Evaluation

The SEM micrographs of Nb7.5Ta tested at room temperature and 400°C are illustrated in Figure 4.11. It is obvious from these micrographs that the morphology of failure was ductile characterized by dimple microstructures. It is, however, interesting to

note that the size of the dimples was larger in the specimen tested at the elevated temperature. The larger dimple size is an indication of increased plasticity at elevated temperatures, thus resulting in higher ductility.

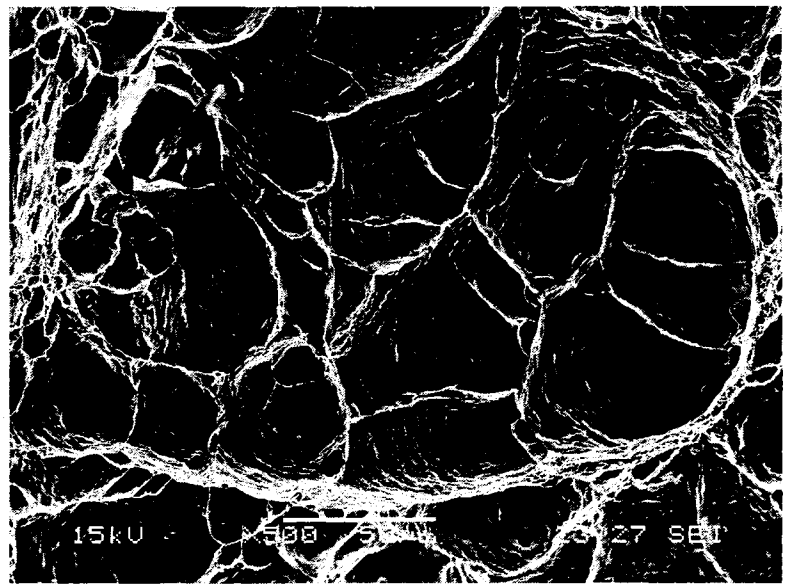

(a) Ambient Temperature

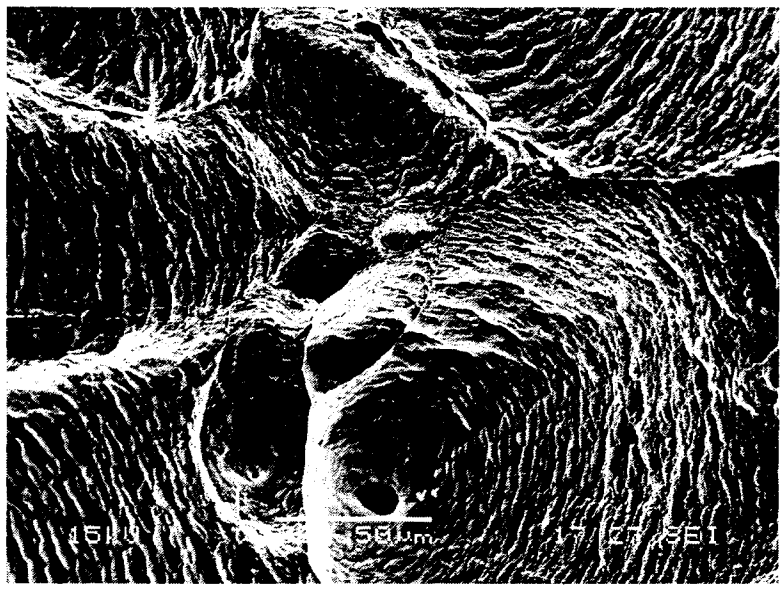

(b). 400°C

Figure 4.11. SEM Micrographs of Tensile Specimens vs. Temperature, 500X

The SEM micrographs of the primary fracture surface of the cylindrical specimens used in the SSR testing are illustrated in Figure 4.12. The SEM micrograph of Nb7.5Ta, tested at room temperature in air, is also included for comparison purpose. An examination of these micrographs reveals that irrespective of the environment and the controlled potential, the nature of failure at the primary fracture surface was ductile showing dimples alone. However, the application of a cathodic E_{cont} (+220mV, Ag/AgCl) resulted in a greater number of microvoids, as shown in Figure 4.12.

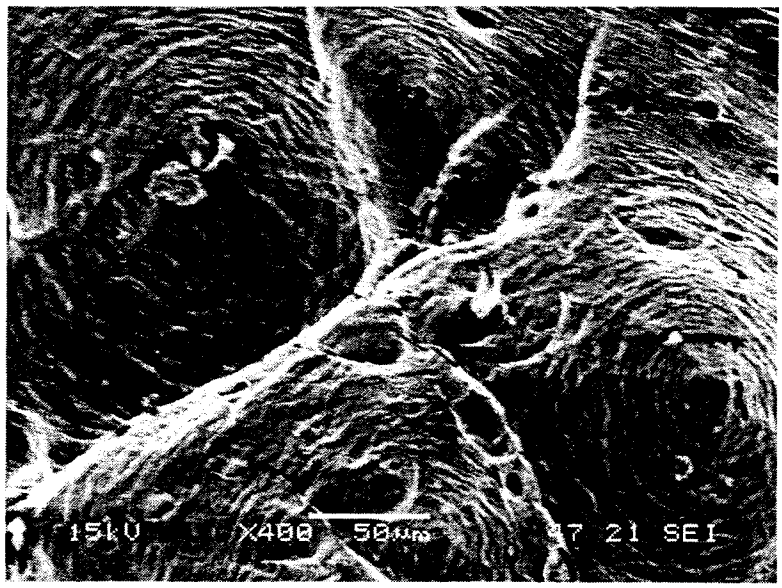

(a). Ambient Temperature, Air

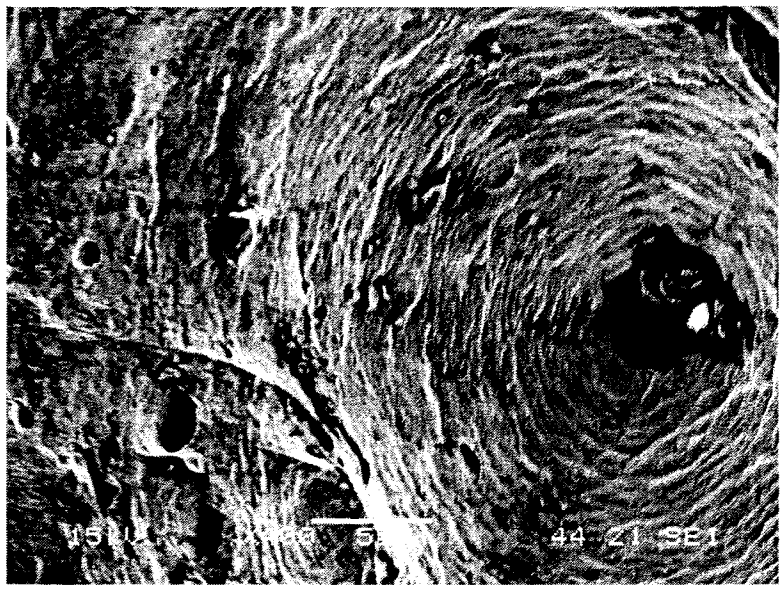

(b). Ambient Temperature, Acidic Solution

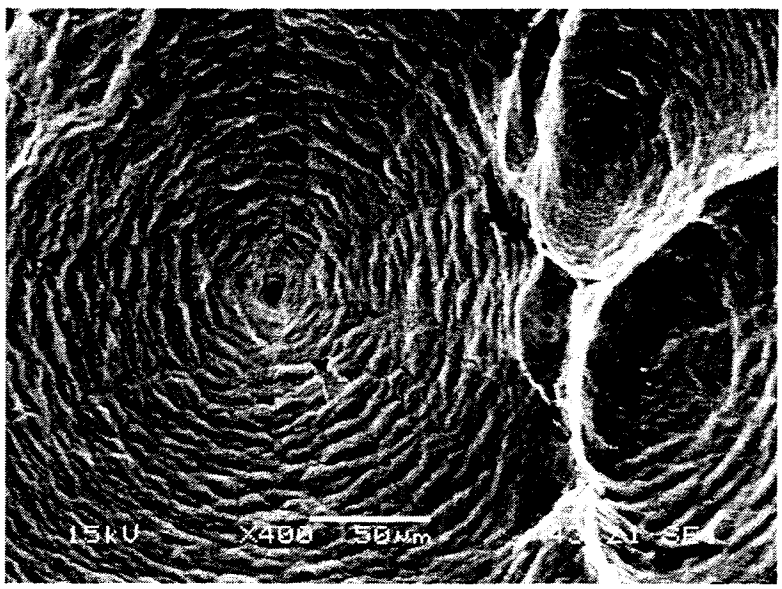

(c). 90°C, Acidic Solution

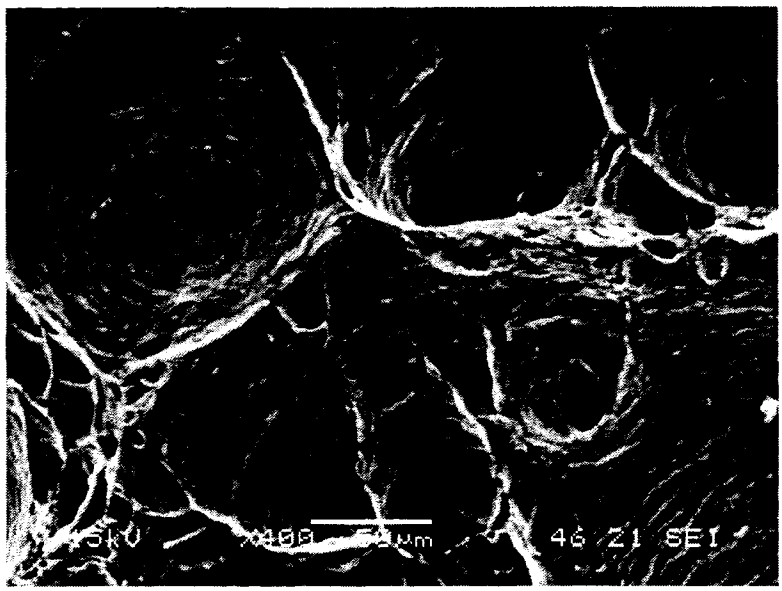

(d). Ambient Temperature, Acidic Solution, E_{cont} = +220 mV

Figure 4.12. SEM Micrographs of SSR Testing

CHAPTER 5

DISCUSSIONS

This investigation has been focused on the characterization of Nb7.5Ta, a leading candidate refractory material for application in nuclear hydrogen generation using the S-I cycle. The refractory materials having lower strength have been proposed for applications during the HI_x decomposition process due to its relatively lower operating temperature compared to that of the sulfuric acid decomposition process. Since a maximum temperature of 400°C has been proposed for the HI_x decomposition process, Nb7.5Ta has been evaluated for its tensile properties at temperatures ranging from ambient to 400°C. The results indicate that this alloy is capable of maintaining a relatively high tensile strength even at 400°C despite its relatively lower room temperature tensile strength.

The tensile data also reveals that the magnitude of the failure strain (e_f) was gradually reduced with increasing temperature ranging from ambient to 300°C. The reduced e_f value in this temperature regime is a manifestation of dynamic strain aging (DSA), which has been reported for many other engineering metals and alloys [25]. The occurrence of DSA in susceptible materials is the result of solute diffusion into the metal lattice, thus impeding the movement of dislocations through individual grains and their boundaries. The dislocation movement is also a function of temperature of plastic deformation. At relatively higher temperatures, beyond the susceptible temperature regime, an engineering metal can experience faster dislocation movement due to its enhanced plastic

flow. A similar phenomenon was noted at 400°C, where the magnitude of plastic strain was enhanced to some extent. Thus, the characterization of dislocation concentration as a function of temperature is of vital importance in developing a mechanistic understanding of DSA phenomenon.

In view of the above rationale, transmission electron microscopy (TEM) was employed to determine dislocation density (ρ) involving tensile specimens tested at ambient temperature, 300 and 400°C. An analysis of the average ρ values based on multiple locations of the TEM micrographs at these temperatures, indicate that the magnitude of ρ was somewhat higher at 300°C compared to that at 400°C. Thus, the relatively lower ρ value at 400°C is consistent with the increased e_f value seen at this temperature in the s-e diagram. As indicated earlier, an enhanced e_f value signifies increased ductility due to the ease of deformation resulting from faster dislocation movement within grains and past the grain boundaries. It is also interesting to note that the magnitude of ρ was reduced by an order at room temperature suggesting that the rate of diffusion of solute elements at this temperature was significantly less. Such reduction in diffusion rate at room temperature can be translated into less resistance to dislocation movements, thus leading to higher e_f value.

The stress corrosion cracking (SCC) testing involving Nb7.5Ta at constant load did not exhibit any failure at ambient and elevated temperatures. However, the cracking susceptibility of this alloy was enhanced in the 90°C acidic solution, showing reduced values of % El, σ_f and TTF indicating a detrimental effect of higher testing temperature (90°C) to promote cracking under a slow strain rate (SSR) condition. With respect to the localized corrosion susceptibility of this alloy, the limited CPP data exhibited E_{corr} and

E_{pit} values of 320 and 900 mV (Ag/AgCl), respectively in an acidic solution at room temperature. A comparison of these data to the critical potential values obtained on NblZr[5] in an identical environment reveals that the current test material is more resistant to dissolution in view of its relatively noble E_{corr} and E_{pit} values. The enhanced resistance of Nb7.5a to localized corrosion can be attributed to the presence of moderate tantalum content. The results of SSR testing involving this alloy under a cathodic E_{cont} value of +220mV (Ag/AgCl) showed reduced failure strain, suggesting a detrimental effect of hydrogen (H) generated from cathodic charging during potentiostatic polarization under tensile loading.

The characterization of the metallurgical microstructures of the tested material by optical microscopy revealed the presence of dark grains of Ta and white grains of Nb, as cited in the open literature. As to the morphology of failure, evaluated by SEM, the primary fracture surface due to tensile loading was characterized by dimples indicating ductile failures. Similarly, the specimens used in the SSR testing exhibited dimpled microstructures, also indicating ductile failures at the primary function surface.

CHAPTER 6

SUMMARY AND CONCLUSIONS

Nb7.5 Ta has been tested for evaluation of its tensile properties at temperatures ranging from ambient to 400°C. The susceptibility of this material to localized corrosion and stress corrosion cracking in an acidic solution has also been evaluated using different state-of-the-art experimental techniques. The metallurgical microstructures of these alloys and the characteristics of failures of the tested specimen have been evaluated by optical microscopy and scanning electron microscopy (SEM), respectively. The significant results derived from this investigation are summarized below

- The tensile data revealed a gradual drop in YS and UTS with increasing temperature resulting from reduced resistance to plastic deformation at elevated temperatures.
- A phenomenon of dynamic strain aging, showing reduced ductility in terms of failure strain (e_f) was noted in the engineering stress vs. strain (s-e) diagram up to a temperature of 300°C. A comparatively higher e_f value was seen at 400°C.
- The TEM micrographs of the tested tensile specimens revealed enhanced clusters of dislocations (ρ) at temperatures up to 300°C, followed by slight reduction at 400°C.
- The magnitude of %EI, σ_f and TTF obtained in SSR testing were significantly reduced in the 90°C acidic solution compared to those at ambient temperature.

- These results demonstrated a detrimental effect of elevated temperature on the cracking susceptibility. No failure was, however, seen at constant load.
- The limited CPP data indicate that Nb7.5 Ta can develop protective oxide films during reverse potential scan, showing a negative hysteresis loop.
- The application of a cathodic controlled potential during SSR testing in an identical acidic solution exhibited reduced failure strain in the s-e diagrams, implying that Nb7.5 Ta may be susceptible to hydrogen embrittlement.
- The evaluation of the fracture morphology by SEM revealed dimpled microstructures in the tensile specimens irrespective of the testing temperature, indicating ductile failures. A similar type of failure was also seen in specimens tested under a SSR condition. However, a greater number of microvoids were observed in the SSR specimen tested under a controlled potential.

CHAPTER 7

FUTURE WORK

- Evaluation of localized corrosion susceptibility at elevated temperatures
- Determination of the cracking susceptibility (SSR) under applied potentials at elevated temperatures
- Evaluation of the stress corrosion cracking tendency using self-loaded specimens at temperatures up to 400°C in an autoclave

APPENDIX A

TENSILE DATA

A1. Stress-Strain Diagrams of Nb7.5Ta Tested at Room Temperature

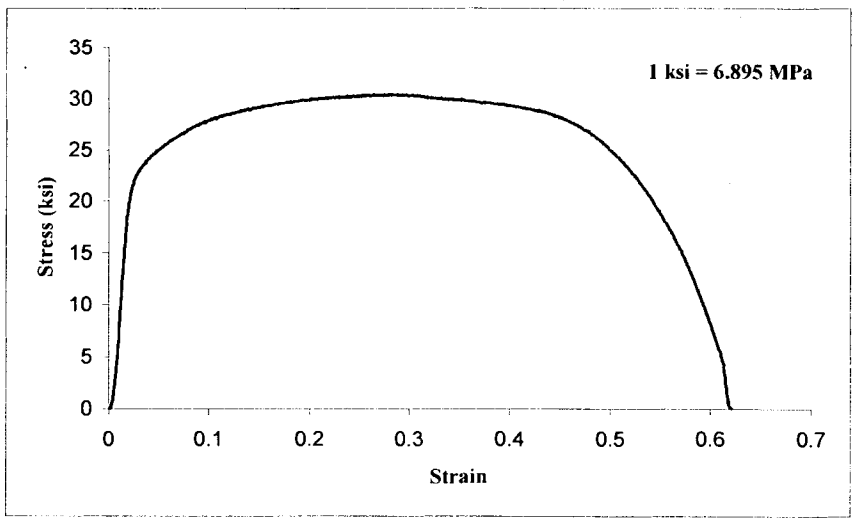

A2. Stress-Strain Diagrams of Nb7.5Ta Tested at 100°C

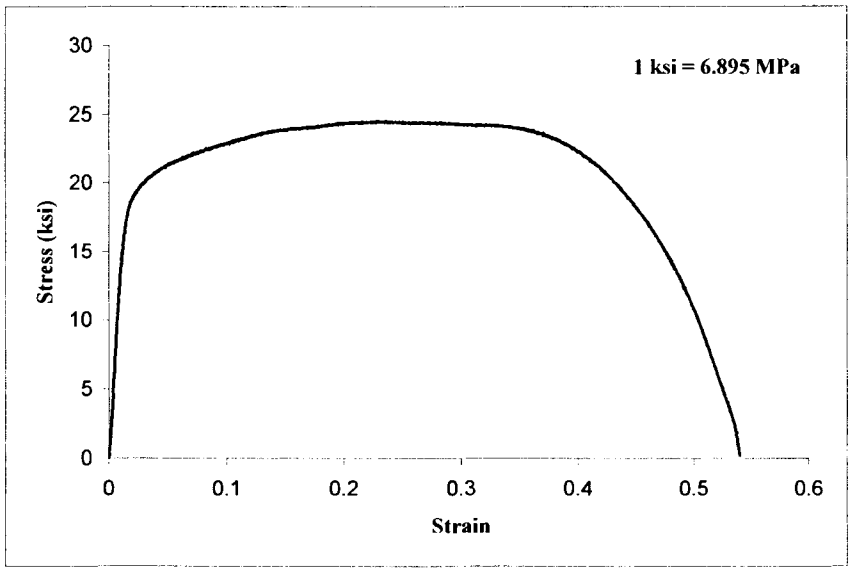

A3. Stress-Strain Diagrams of Nb7.5Ta Tested at 200°C

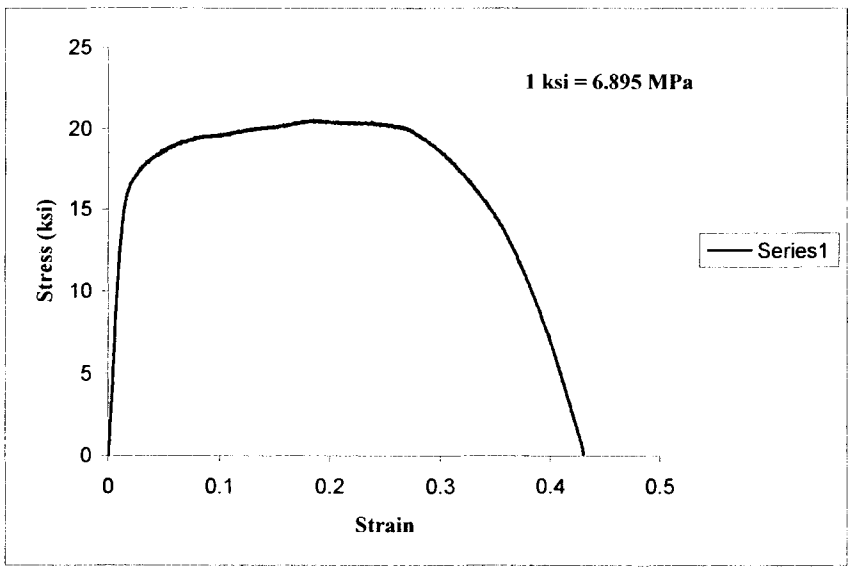

A4. Stress-Strain Diagrams of Nb7.5Ta Tested at 300°C

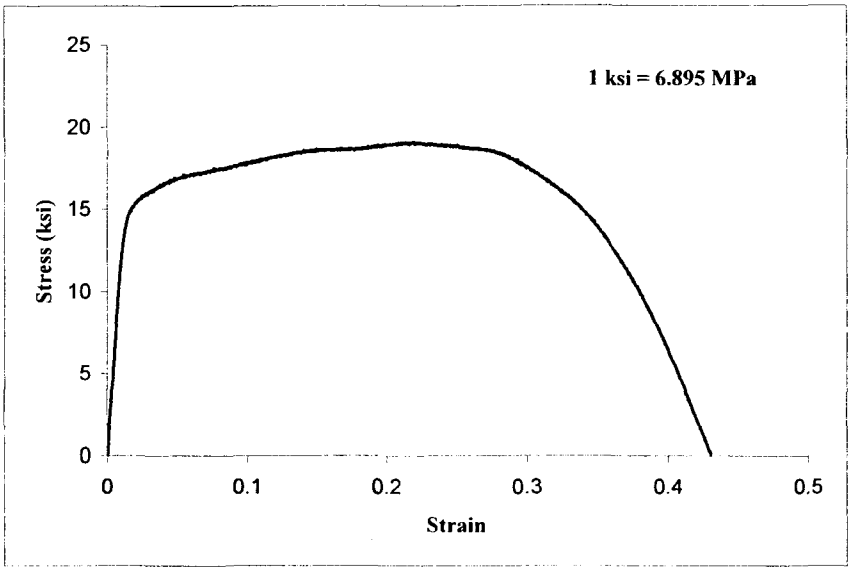

A5. Stress-Strain Diagrams of Nb7.5Ta Tested at 400°C

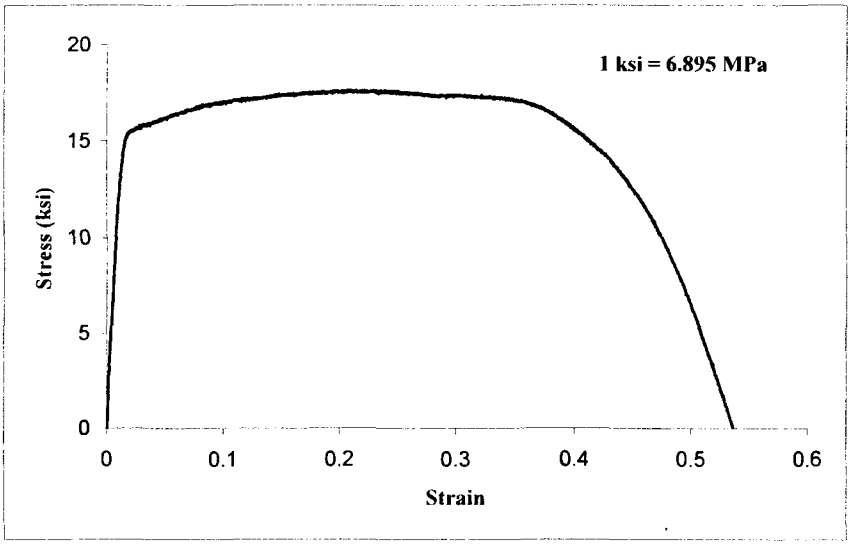

APPENDIX B

SLOW-STRAIN-RATE DATA

B1. Stress – Strain Diagrams in Air using Smooth Specimens for Nb7.5Ta at Room Temperature

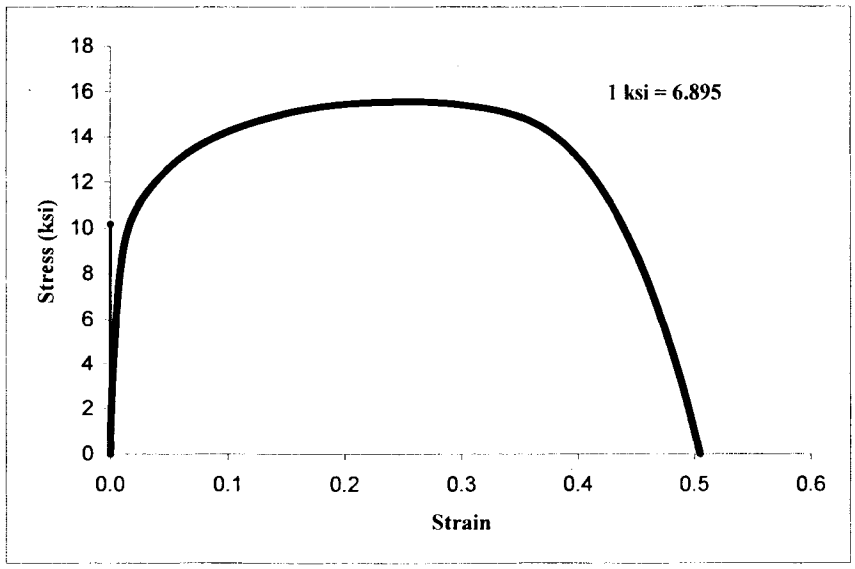

B2. Stress – Strain Diagrams in acidic solution using Smooth Specimens for Nb7.5Ta at Room Temperature

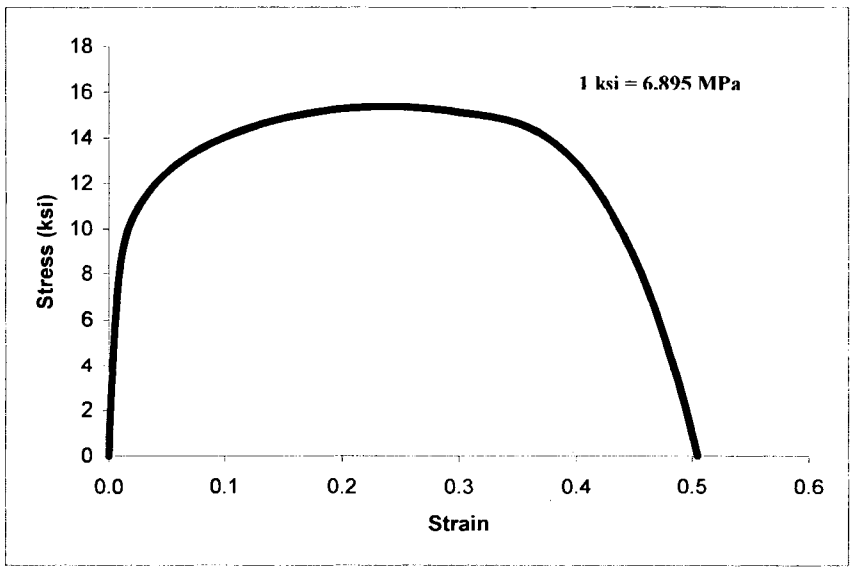

B3. Stress – Strain Diagrams in acidic solution using Smooth Specimens for Nb7.5Ta at 90°C

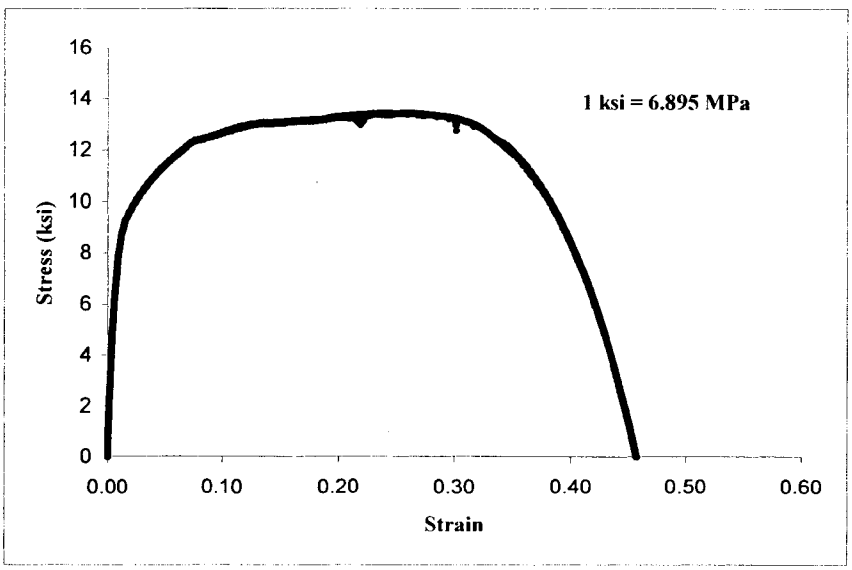

APPENDIX C

CPP TEST DATA

C1. CPP Diagram for Nb7.5Ta at 30°C

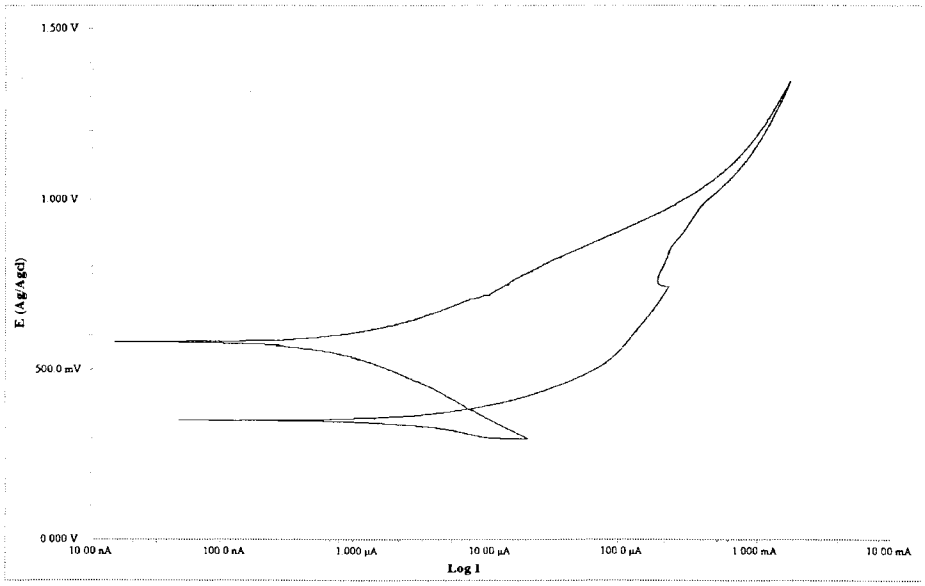

APPENDIX D

SSR UNDER CATHODIC CONTROLLED POTENTIAL DATA

D1. E_{cont} at +220 mV

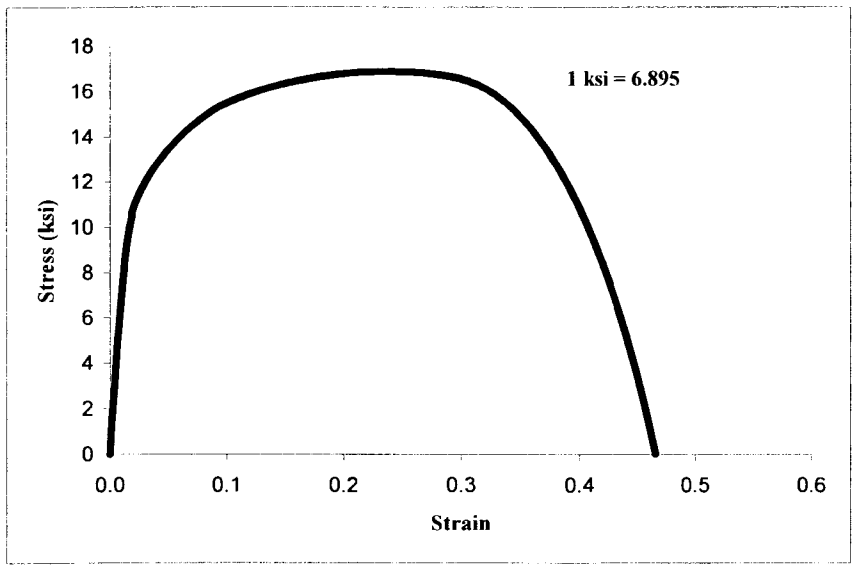

APPENDIX E

SEM MICROGRAPHS

E1. SEM Micrographs of Nb7.5Ta at Room Temperature, MTS

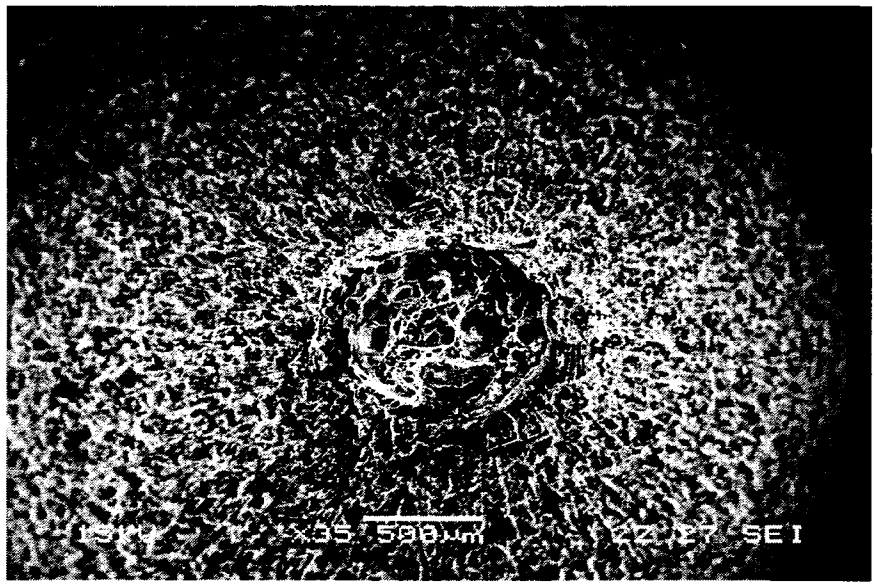

Magnification - 35X

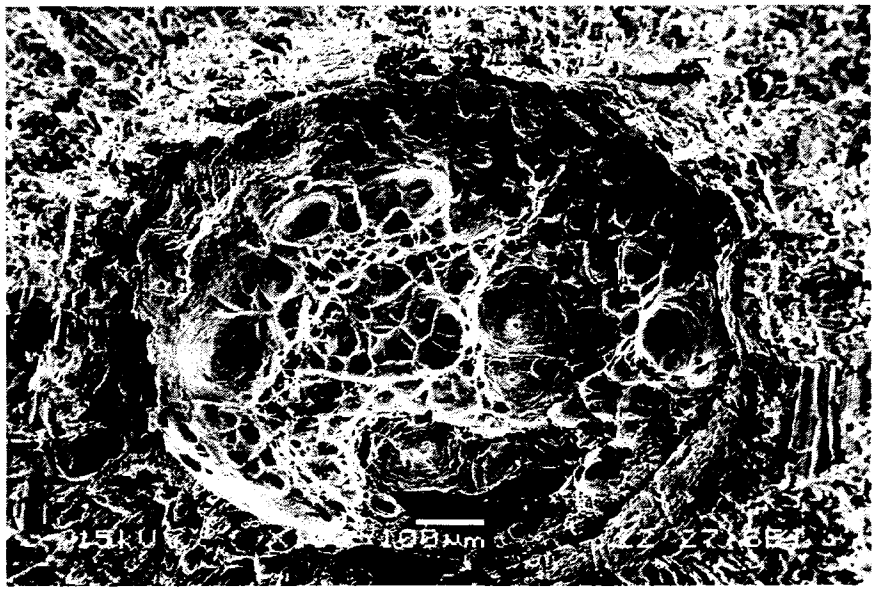

Magnification - 100X

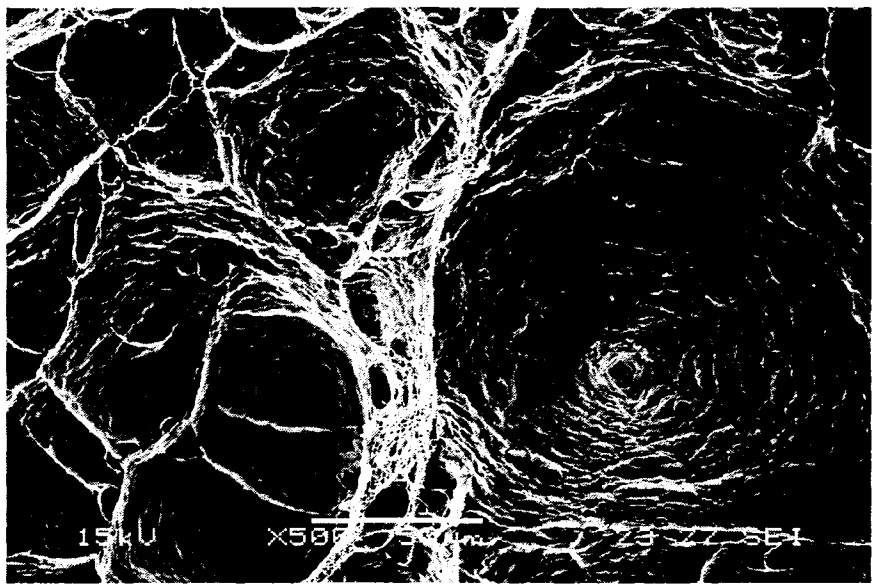

Magnification - 500X

E2. SEM Micrographs of Nb7.5Ta at 400°C, MTS

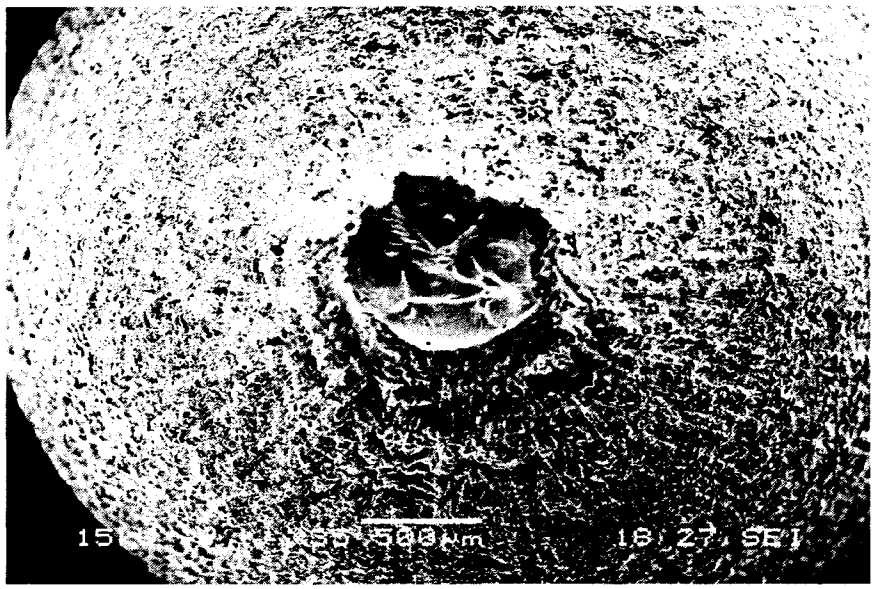

Magnification - 35X

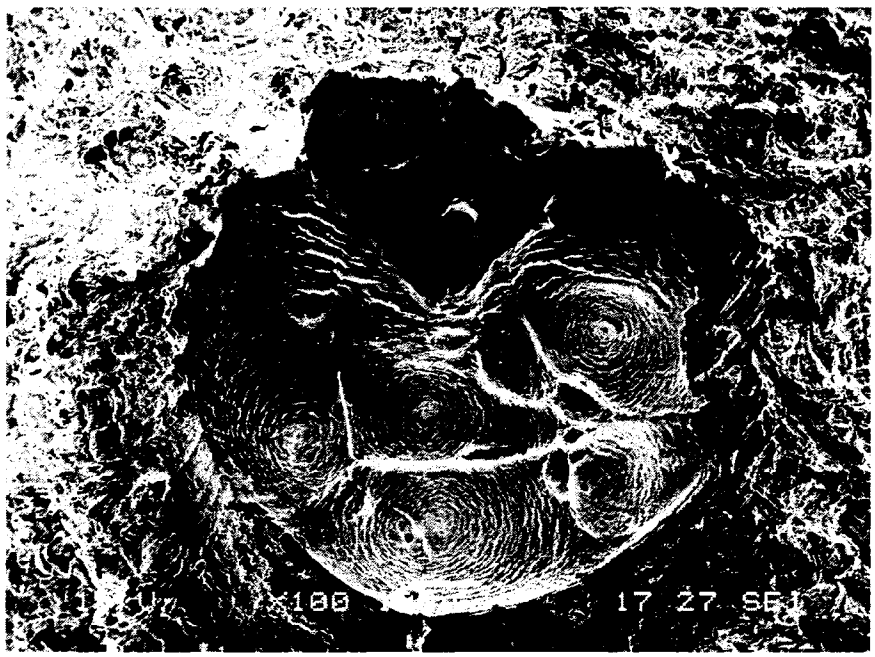

Magnification - 100X

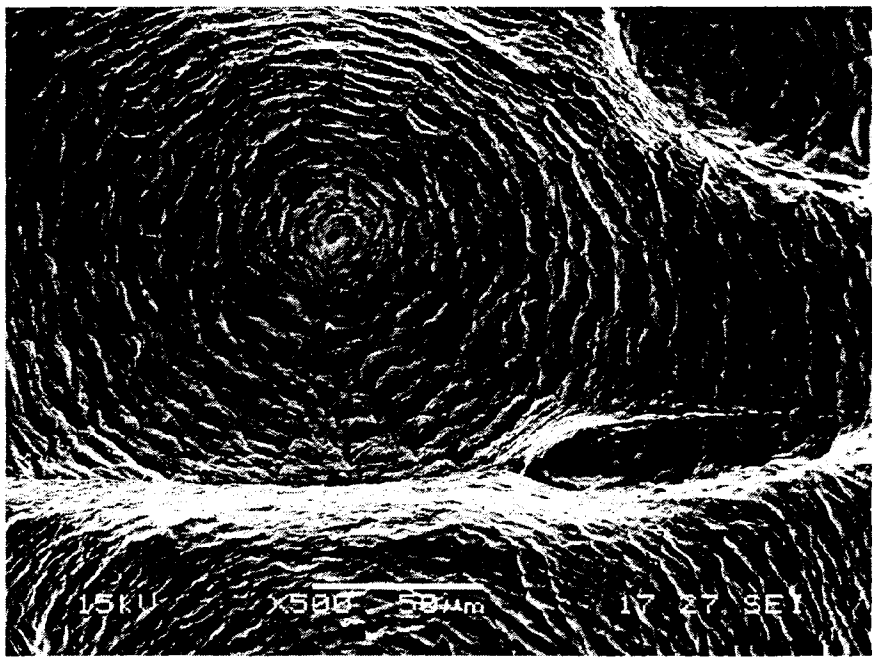

Magnification - 500X

APPENDIX F

TEM MICROGRAPHS

F1. TEM Micrographs of Nb7.5Ta at Room Temperature

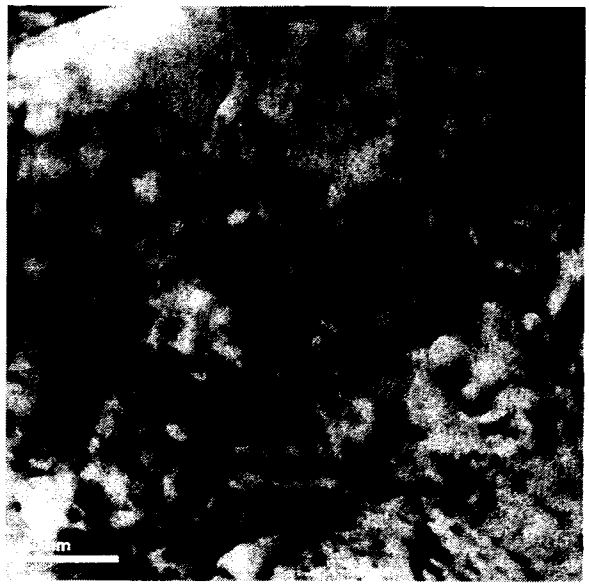

Magnification 120K

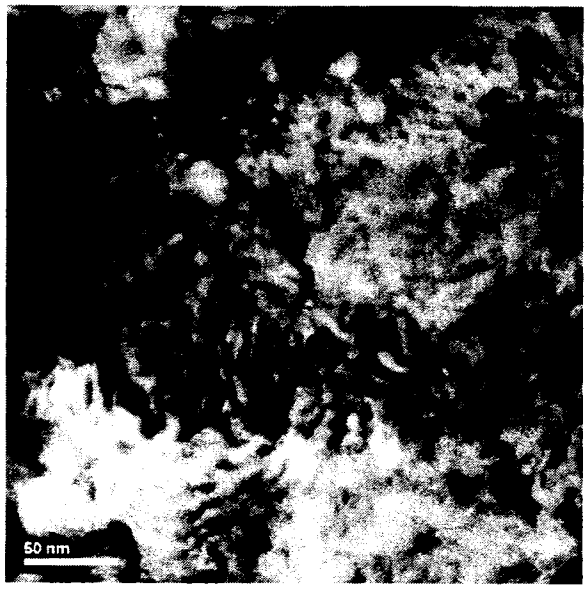

Magnification 120K

F2. TEM Micrographs of Nb7.5Ta at 300°C

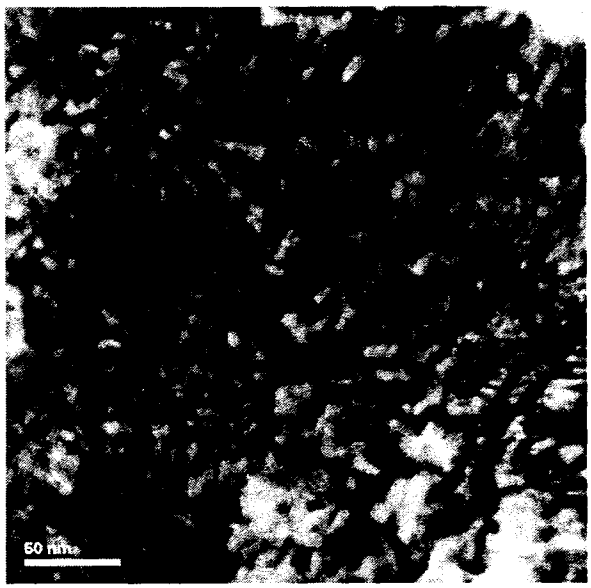

Magnification 120K

Magnification 250K

F2. TEM Micrographs of Nb7.5Ta at 400°C

Magnification 120K

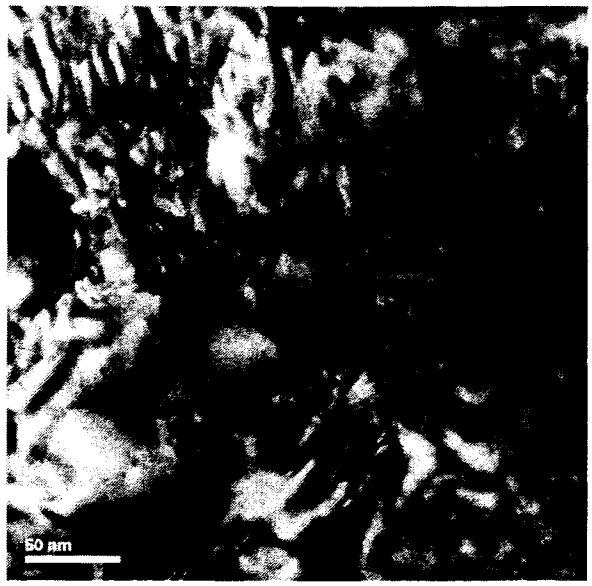

Magnification 400K

APPENDIX G

UNCERTAINITY ANALYSES

Uncertainity is a parameter, associated with the result of a measurement (eg. a calibration or test) that defines the range of the values that could reasonably be attributed to the measured quantity. When uncertainty is evaluated and reported in a specified way it indicates the level of confidence that the value actually lies within the range defined by the uncertainty interval. Any measurement is subject to imperfections; some of these are due to random effects, such as short-term fluctuations in temperature, humidity and air-pressure or variability in the performance of the measurer. Repeated measurements will show variation because of these random effects. Other imperfections are due to the practical limits to which correction can be made for systematic effects, such as offset of a measuring instrument, drift in its characteristics between calibrations, personal bias in reading an analogue scale or the uncertainty of the value of a reference standard. A proper evaluation of uncertainty can provide laboratories with valuable information about the quality and reliability of the result.

In order to reduce the amount of uncertainty, all the experimental setups at Materials Performance Laboratory were calibrated on a timely basis. A precise method described by Kline and McClintock [26] is used to calculate the uncertainties of different temperatures. The method is based on a careful specification of the uncertainties in the various primary experimental measurements. The maximum load-cell reading of the

slow-strain-rate (SSR) experimental setup is 7500 lbs ± 0.3% lbs. The reading on the load scale is thus uncertain to some extent which is expressed as a deviation either in the positive side or the negative side from the standard maximum value. As discussed earlier, the level of uncertainty is dependent on the calibration standard. Calibration of instruments using high precision standards will lead to lower level of uncertainty compared to the calibration performed with gages or instruments of unknown calibration.

All the experimental setups in the Materials Performance Laboratory (MPL) were calibrated using standards, with a very high precision, on a regular basis by Bechtel Nevada. Thus, it is expected that the resultant data presented would have low uncertainties. The uncertainties in the results of this investigation are calculated by using the Kline and McClintock Method. The equation used for this method is given below.

$$W_R = \left[\left(\frac{\partial R}{\partial x_1} w_1 \right)^2 + \left(\frac{\partial R}{\partial x_2} w_2 \right)^2 + \cdots + \left(\frac{\partial R}{\partial x_n} w_n \right)^2 \right]^{\frac{1}{2}} \quad \text{.....(G.1)}$$

Where, W_R = the uncertainty in the results

R = the given function of the independent variables $x_1, x_2, \ldots x_n$)

$R = R(x_1, x_2, \ldots x_n)$

$w_1, w_2, \ldots w_n$ = the uncertainty in the independent variables

G1 Uncertainty Calculation for Parameters Derived from MTS Results

The results obtained from the MTS testing includes, stress (σ), percent elongation (%El), and percent reduction in area (%RA). The stress is based on the load (P) and the initial cross-sectional area (A_i) of the tested specimen. The %El is calculated based on the change in length (Δl) during the testing according to the equation 3.1 and the %RA is calculated based on the initial and final cross-sectional areas (A_i and A_f) of the tested specimen according to the equation 3.2. The magnitude of P was obtained from the load-cell of the MTS unit. However, the values for Δl, A_i, and A_f were calculated based measurements by a caliper. The uncertainties in load-cell and caliper were ± 0.03% lbs and ± 0.001 in, respectively, obtained from the calibration.

G1.1 Calculation of Uncertainty in Stress ($_u\sigma$)

$_u\sigma = {}_u(P, A_i)$

$_uA_i = (uD_i)^2$

Uncertainty in load-cell = ± 0.03% lb

Uncertainty in caliper = ± 0.001 in

Sample calculation:

For yield stress (YS) = 21.29 ksi

Uncertainty in load ($_uP$) = 1043.21*0.0003

= ± 0.3129

Uncertainty in cross-sectional area ($_uA_i$) for the smooth specimen:

Initial Diameter (D_i) = 0.25 in

Uncertainty in diameter ($_uD$) $= \pm 0.001$ in

$$\text{Area } (A_i) = \frac{\pi D_i^{\,2}}{4}$$

$$= 0.049$$

$$\frac{dA_i}{dD_i} = \frac{\pi D_i}{2}$$

$$= 0.393$$

$$\text{Uncertainty in area, } {}_u A_i = \left[\left(\frac{dA_i}{dD_i} \cdot {}_u D_i\right)^2\right]^{\frac{1}{2}}$$

$$= 0.393 * 0.001$$

$$= \pm 0.000393$$

$$\text{Uncertainty in stress, } {}_u\sigma = \left[\left(\frac{\partial\sigma}{\partial P} \cdot {}_u P\right)^2 + \left(\frac{\partial\sigma}{\partial A_i} \cdot {}_u A_i\right)^2\right]^{\frac{1}{2}} \quad \text{..... (G.2)}$$

$$\sigma = \frac{P}{A_i}$$

$$\frac{\partial\sigma}{\partial P} = \frac{1}{A_i}$$

$$= 20.41$$

$$\frac{\partial\sigma}{\partial A_i} = -\frac{P}{A_i^{\,2}}$$

$$= -1081632.65$$

Now providing all the numerical values in equation (G.2) obtained from the calculation, it is found that,

$${}_u\sigma = \left[(20.41 * 0.3129)^2 + (-434490 * 0.000393)^2\right]^{\frac{1}{2}}$$

$= 170.8$ psi

$= \pm 0.17$ ksi

G1.2 Calculation of Uncertainty in Percentage Elongation ($_u$%El)

Sample calculation:

Change in length (Δl) $= 0.56$ in

Gage length (l) $= 1$ in

$$\%El = \frac{\Delta l}{l} \cdot 100$$

Uncertainty in Δl ($_u\Delta l$) $= \pm 0.001$

Uncertainty in %El ($_u$%El),

$$_u\%El = \left[\left(\frac{d\%El}{d\Delta l} \cdot {}_u\Delta l\right)^2\right]^{\frac{1}{2}} \quad \text{..... (G.3)}$$

$$\frac{d\%El}{d\Delta l} = \frac{100}{l}$$

$= 100$

Providing all the calculated values in equation G.3, it is found that,

$$_u\%El = \left[(100 * 0.001)^2\right]^{\frac{1}{2}}$$

$_u$%El $= \pm 0.1$

G2 Uncertainty Calculation in Slow-Strain-Rate (SSR) Testing

G2.1 Uncertainty Calculation in True Failure Stress ($_u\sigma_f$)

The uncertainty in the σ_f is based on the failure load (P_f) and the final cross-sectional area (A_f) of the tested specimen. The uncertainty in the σ_f was calculated based on the P_f and A_f using the equation G.2.

G2.2 Uncertainty Calculation in Percentage Elongation ($_u$%El)

The uncertainty in the %El was calculated using the equation G.3.

G2.3 Calculation of Uncertainty in Percentage Reduction in Area ($_u$%RA)

Sample calculation:

For %RA = 96.9%

Uncertainty in initial cross-sectional area ($_uA_i$) for the smooth specimen:

Initial Diameter (D_i) = 0.25 in

Uncertainty in initial diameter,

$$(_uD_i) = \pm 0.001 \text{ in}$$

$$\text{Area } (A_i) = \frac{\pi D_i^2}{4}$$

$$= 0.049$$

$$\frac{dA_i}{dD_i} = \frac{\pi D_i}{2}$$

$$= 0.393$$

Uncertainty in initial cross-sectional area,

$$ {}_u A_i = \left[\left(\frac{dA_i}{dD_i} \cdot {}_u D_i \right)^2 \right]^{\frac{1}{2}} $$

$$ = 0.393 * 0.001 $$

$$ = \pm 0.000393 $$

Uncertainty in final cross-sectional area (U_{Af}) for the smooth specimen:

Final Diameter (D_f) = 0.044in

Uncertainty in final diameter (UD_f),

$$ = \pm 0.001 \text{ in} $$

$$ \text{Area } (A_f) = \frac{\pi D_f^{\,2}}{4} $$

$$ = 0.0015 $$

$$ \frac{dA_f}{dD_f} = \frac{\pi D_f}{2} $$

$$ = 0.0015 $$

Uncertainty in final cross-sectional area,

$$ {}_u A_f = \left[\left(\frac{dA_f}{dD_f} \cdot {}_u D_f \right)^2 \right]^{\frac{1}{2}} $$

$$ = 0.0015 * 0.001 $$

$$ = 0.0000015 $$

Uncertainty in ${}_u$%RA,

$$ {}_u \%RA = \left[\left(\frac{\partial \%RA}{\partial A_i} \cdot {}_u A_i \right)^2 + \left(\frac{\partial \%RA}{\partial A_f} \cdot {}_u A_f \right)^2 \right]^{\frac{1}{2}} \quad \text{..... (G.4)} $$

$$\%RA = \left(\frac{A_i - A_f}{A_i}\right) * 100$$

$$= \left(1 - \frac{A_f}{A_i}\right) * 100$$

$$\frac{\partial \%RA}{\partial A_i} = \frac{100 A_f}{A_i^2}$$

$$= 971.2$$

$$\frac{\partial \%RA}{\partial A_f} = -\frac{100}{A_i}$$

$$= -2471.25$$

Now assigning all the calculated values in equation G.4, it is found that,

$$_u\%RA = \left[(971.1 * 0.000393)^2 + (-2471.25 * 0.0000015)^2\right]^{\frac{1}{2}}$$

$$= 0.146$$

One example of the use of the uncertainty analysis is shown in this section. This can be implemented to all experimental results discussed in this thesis.

G2.4 Uncertainty Calculation in Time-To-Failure (TTF)

The TTF is obtained from the Filed Point software of the slow-strain-rate (SSR) unit, which is accurate up to $\frac{1}{100}$th of a second in finding the TTF. Therefore, the uncertainty of the TTF in the SSR testing is negligible.

G3 Uncertainty Calculation in Cyclic Potentiodynamic Polarization (CPP) Testing

The accuracy of the potentiostat provided by the manufacturer is ± 0.003 mV within a range of 1 mV.

Sample calculation: For corrosion potential (E_{corr}) = 288 mV

The uncertainty in E_{corr} = 288*0.003

= ± 0.864 mV

BIBLIOGRAPHY

1. Bilge Yildiz, Mujid S. Kazimi, "Efficiency of hydrogen production systems using alternative nuclear energy technologies," *International Journal of Hydrogen Energy*, Article in press.
2. http://hydrogen.kaist.ac.kr/gen_01.php?menu_type=gen
3. D. O'keefe, C. Allen, G. Besenbruch, L.Brown, J. Norman, R. Sharp, "Preliminary results from bench-scale testing of a sulfur-iodine thermochemical water- splitting cycle," International Journal of Hydrogen Energy, Vol. 7, No.5, 1982, pp. 381 – 392.
4. Radhakrishnan Santhanakrishnan, " Metallurgical and corrosion characterization of structural materials for S-I cycle," M.S. Thesis, Department of Mechanical Engineering, University of Nevada, Las Vegas, December 2005.
5. Ancila V. Kaiparambil, "Characterization of structural materials for applications in HI_x decomposition," M.S.Thesis, Department of Mechanical Engineering, University of Nevada, Las Vegas, December 2005.
6. http://www.welding-advisers.com/Refractory-metals.html
7. Wojcik, C. Craig, "Processing, properties and applications of high-temperature niobium alloys," *Materials Research Society symposia proceedings*, Vol. 322, 1994, pg. 519-530.
8. Vani Shankar, M. Valsan, K. Bhanu Shankar Rao and S.L. Mannan, "Effects of Temperature and Strain Rate on Tensile Properties and Activation Energy for Dynamic Strain Aging of Alloy 625".

9. Niobium, www.cabot-corp.com

10. Tantalum, www.cabot-corp.com

11. ASTM Designation E 8 (04), "Standard Test Methods for Tension Testing of Metallic Materials," *American Society for Testing and Materials (ASTM) International.*

12. Paul E. Fischione – Materials Specimen Preparation for Transmission Electron Microscopy, E.A.Fishione Instruments, Inc.Export, PA USA

13. Loretto MH., Electron beam analysis of materials, London: Chapman and Hall, 1994.

14. J. Pesicka, R. Kuzel, A. Dronhofer, G. Eggeler, Acta Materialia, Vol. 51, 2003, pp. 4847-4862.

15. R. F. Egerton., Electron Energy Loss Spectroscopy in the Electron Microscope, Plenum Press, 1986, pp. 291-352.

16. Corrosion Testing Equipment, Cortest, Incorporated. www.cortest.com

17. ASTM Designation G129-2000, "Standard Practice for Slow Strain Rate Testing to Evaluate the Susceptibility of Metallic Materials to Environmentally Assisted Cracking," *American Society for Testing and Materials (ASTM) International.*

18. A. K. Roy, et al., "Effect of Controlled Potential on SCC of Nuclear Waste Package Container Materials," *Proceedings of NACE Corrosion 2000*, Paper No. 00188, Orlando, FL, 2000

19. A.K. Roy, et al., "Stress Corrosion Cracking of Ni-Base and Ti Alloys Under Controlled Potential," 7th *International Conference on Nuclear Engineering*, Paper No. ICONE-7048, Tokyo, Japan, April 19-23, 1999

20. A.K. Roy, et al., "Cracking of Titanium Alloys under Cathodic Applied Potential," *Micron, Elsevier Science*, Vol 32, No.2, pp. 211-218, Feb 2001.

21. Gamry Instruments. http://www.gamry.com/Homepage/CorrosionPage.htm

22. ASTM Designation G 5-94 (1999) e1, "Standard Reference Test Method for Making Potentiostatic and Potentiodynamic Anodic Polarization Measurements," *American Society for Testing and Materials (ASTM) International.*

23. Hirsch P, Howie A, Nicholson R, Pashley DW, Whelan MJ., Electron microscopy of thin crystals, Malabar: Krieger Publishing company, 1977 optical

24. E.V.Vasilleva, D.A. Prokoshkin, "Structure and Some Properties of Niobium – Tantalum Alloys Containing Tungsten and Molybdenum," Institute of Metallurgy.

25. Subhra Bandhyopadhyay., "Residual Stress Characterization and Defect Analyses by Microscopy". M.S.Thesis, Department of Mechanical Engineering, University of Nevada, Las Vegas, December 2005.

26. Jack P. Holman, "Experimental Methods for Engineers," McGraw-Hill Book Company, 4th Edition, pp. 50

VITA

Graduate College
University of Nevada, Las Vegas

Venkateswarlu Kondur

Address:

4213 Grove Circle, Apt # 1,
Las Vegas, NV, 89119, USA,

Degree:
Bachelor of Technology, Mechanical Engineering, 2003
J.N.T.U, Hyderabad, India

Special Honors and Awards:

- Member of Tau Beta Pi.
- Awarded Graduate Assistantship at UNLV to pursue M.S. program in Mechanical Engineering.
- Received Best Student Award in High School.

Thesis Title: "Characterization of Nb7.5Ta for HI_x Decomposition Process".

Thesis Examination Committee:
Chairperson, Dr. Ajit K. Roy, Ph.D.
Committee Member, Dr. Anthony E. Hechanova, Ph.D.
Committee Member, Dr. Daniel P. Cook, Ph.D.
Graduate College Representative, Dr. Edward S. Neumann, Ph.D.